SAR and InSAR data linked to soil moisture changes on a temperate raised peatland subjected to a wildfire

Alexis Hrysiewicz[1,2,*], Eoghan P. Holohan[1,2], Shane Donohue[1,3] and Hugh Cushnan[4]

[1]SFI Research Center in Applied Geosciences (iCRAG), University College Dublin, Belfield, Dublin 4, Ireland

[2] UCD School of Earth Sciences, University College Dublin, Belflied, Dublin 4, Ireland

[3] UCD School of Civil Engineering, University College Dublin, Belflied, Dublin 4, Ireland

[4] RPS Group, Elmwood House, 74 Boucher Road, Belfast, BT12 6RZ Northern Ireland, United Kingdom

Corresponding author: Alexis Hrysiewicz (alexis.hrysiewicz@ucd.ie)

SAR and InSAR data linked to soil moisture changes on a temperate raised peatland subjected to a wildfire

Alexis Hrysiewicz[1,2,*], Eoghan P. Holohan[1,2], Shane Donohue[1,3] and Hugh Cushnan[4]

[1]SFI Research Centre in Applied Geosciences (iCRAG), University College Dublin, Belfield, Dublin 4, Ireland

[2] UCD School of Earth Sciences, University College Dublin, Belflied, Dublin 4, Ireland

[3] UCD School of Civil Engineering, University College Dublin, Belflied, Dublin 4, Ireland

[4] RPS Group, Elmwood House, 74 Boucher Road, Belfast, BT12 6RZ Northern Ireland, United Kingdom

Corresponding author: Alexis Hrysiewicz (alexis.hrysiewicz@ucd.ie)

Highlights

- InSAR time-series analysis for measurement of ground motion on a raised peatland.
- InSAR is critically influenced by soil moisture changes and temporal baselines.
- Short-term coherence (< 1 year) is mainly controlled by soil moisture changes.
- A wildfire on the raised peatland affected SAR intensity but not InSAR measurements.
- SAR backscatter intensity and InSAR phase represent different parts of the peat column.

Abstract

Interferometry of Synthetic Aperture Radar (InSAR) can potentially contribute to the cost-effective regional or global monitoring of the degradation and restoration of peatlands. However, there are uncertainties about the links between InSAR results and peatland ecohydrological parameters, especially soil moisture. Here, we analyse the relationships between the temporal evolutions of InSAR coherence, ground displacements, and in-situ soil moisture measurements for a temperate raised bog at Ballynafagh, Co. Kildare, Ireland, in the period 2017-mid-2021. We also investigate the effects of a wildfire in June-July 2019 on those relationships. InSAR-derived ground displacements from Sentinel-1 C-band radar data indicate long-term subsidence of the intact and Active Raised Bog. Superimposed on the long-term displacement trends are annual oscillations that are linked to variations in rainfall and temperature and that are in phase with changes in soil moisture. We show that InSAR coherence is directly related to the change in soil moisture, with large changes causing coherence decrease or loss. The wildfire removed a 10-20 cm thick mossy vegetation layer across 60-70 % of the intact bog area. The SAR backscatter intensity in VV polarisation increased after the wildfire, but the InSAR coherence, the InSAR-derived surface displacements and the soil moisture were not noticeably affected. We therefore infer that C-band radar waves attenuate in the active vegetation layer, but penetrate through it into the upper few cm of the underlying peat. The SAR backscatter occurs primarily at this level in the peat, where its coherence is controlled by the soil moisture. These findings underpin application and interpretation of radar for monitoring of peatlands, even if affected by wildfires, which are forecast to increase in both frequency and intensity due to global warming.

1. Introduction

Peatlands are one of the largest carbon sinks on Earth: an estimated 20-30 % of global soil carbon is to be stored in peat, despite fens and bogs covering only a small percentage of the world's land surface (Drösler et al., 2008; Gorham, 1991; Köchy et al., 2015; Renou-Wilson et al., 2019; Yu et al., 2010). However, the role of peatlands in greenhouse-gas (GHG) emissions on global emissions is still unknown or poorly quantified, and so closing this knowledge gap has been become a priority in the context of mitigating global warming (Hiraishi et al., 2014; Leifeld & Menichetti, 2018; Roulet, 2000). In addition, peatland restoration is a focus of current mitigation efforts, (Renou-Wilson et al., 2019), both to maintain the capacity of peatland to be GHG sinks, and also to preserve their endemic flora and fauna, (Parish et al., 2008). Peatlands have been monitored traditionally through in-situ measurements of various key ecohydrological parameters, (e.g., ground level, soil moisture, temperature, groundwater levels, water balance, etc.) and GHG emissions. However, our ability to extend such monitoring of peatlands to regional, national or global scales is a challenge. In Ireland, for example, approximately 15 % of the island – c. 12,700 out of 84,400 km^2 - is covered by peat soils (Connolly & Holden, 2009). Globally, 2.84 % of the world land area, amounting to 4.23 million km^2, is peatland (Xu et al., 2018).

Spatial remote sensing has complemented in-situ measurements, providing quantification of peatlands over large areas for several years, (e.g., Connolly & Holden, 2009; Connolly et al., 2007; Jones et al., 2009). Satellite data allow estimates of many ecohydrological parameters to be processed, with worldwide coverage, high accuracy and low cost (data being increasingly open-source and free of charge to end-user), (Lees et al., 2018). Most past remote-sensing work on peatlands has involved passive approaches such as optical, multispectral and hyperspectral imaging, as well as active approaches such as LiDAR (Minasny et al., 2019) and Synthetic Aperture Radar

(SAR). SAR images, which are the focus of this work, contain information on the amplitude and phase of backscatter radar signal. Previous work on peatlands has mainly focussed on the signal amplitude (or intensity). For example, methods using the backscatter intensity of synthetic aperture radar (SAR) have been developed to estimate soil moisture at medium spatial resolutions (~1 km), (e.g., Balenzano et al., 2012; Balenzano et al., 2021; Paloscia et al., 2013; Peng et al., 2021; Wagner et al., 2013), and have been generalised to peat soil parameters (i.e., peat conditions, soil moisture, groundwater levels), (Asmuß et al., 2018; Bechtold et al., 2018; Kim et al., 2017; Millard & Richardson, 2018; Millard et al., 2018; Takada et al., 2009).

In recent years, Interferometry of Synthetic Aperture Radar (InSAR), which uses the phase information in SAR images, has been used to estimate peat surface displacements (Alshammari et al., 2020; Fiaschi et al., 2019). Such displacements are known from ground data to be linked to changes in peatland ecohydrological conditions, especially water table levels, and carbon emissions (Evans et al., 2021; Regan et al., 2019). Indeed, peatland surface motions comprise both annual oscillations - termed 'bog'- or 'mire-breathing' - and multi-annual to decadal subsidence linked with sustained ground water level fall (Alshammari et al., 2018; Reeve et al., 2013). For tropical peatlands, this has led to newly proposed methods for estimating GHG emissions on very large scales from InSAR data, (Hoyt et al., 2020; Zhou, 2013; Zhou et al., 2016). InSAR coherence is a second product of InSAR that describes the quality of the phase information. Coherence also has recently emerged as an alternative means of estimating soil moisture, (De Zan & Gomba, 2018; Zwieback et al., 2015b), although this appears to be complex and statically unsustainable on conventional soils, (Eshqi Molan & Lu, 2020a).

Ostensibly, peatlands are an unusual target for the successful use of InSAR time-series methods to derive surface displacement. Vegetated target areas are prone to strong decorrelation of the radar phase over successive radar acquisitions, (Zebker & Villasenor, 1992). This is especially problematic at shorter radar wavelengths (e.g. X-band or C-band), for which penetration of the vegetation by the radar waves is progressively inhibited. Decorrelation in such areas is linked to transient backscattering conditions in the vegetation and/or to variations in underlying soil properties, especially soil moisture (Nesti et al., 1995). Peatlands such as raised bogs or blanket bogs are characterised by a relatively thin (5-50 cm) active vegetation layer, referred as the acrotelm, which when in good condition is dominated by sphagnum mosses. Such vegetation could present more stable backscattering dynamics than other vegetation types (e.g. grasslands), and thus be a factor in the unusually high coherence at peatlands (Millard et al., 2020). On the other hand, coherence at peatlands has been noted to decline during seasonal dry periods as the groundwater table declines (Tampuu et al., 2020). InSAR-derived displacements on peatlands (Marshall et al., 2022; Tampuu, 2022) have been validated in part by levelling, although with the caveat that displacements during dry summer periods may be underestimated. Thus soil moisture could exert a complementary or overriding control on coherence, but links between in-situ soil moisture measurements and InSAR data have been lacking.

A further complication is that peatlands can be affected by wildfires. Depending on burn duration and intensity, wildfires can cause significant damage to both the active vegetation and the underlying peat**,** (Wilkinson et al., 2020). In this case, wildfires can potentially change a peatland's ecohydrological state and its ability to sequester carbon (Kettridge et al., 2012; Reddy et al., 2015)**.** For example, Hooijer et al. (2014) defines different relationships between GHG emissions and peatland surface displacements depending on peat conditions (burnt, drained, etc.). Khakim et al. (2020) also shows an increase in peatland subsidence after severe wildfire on tropical peatlands. Understanding of the impact of wildfire on InSAR results for peatlands is thus important for both application and interpretation, but to date has received little if any attention.

In this study, we analyse C-band satellite InSAR products, including coherence maps, temporal evolutions of displacements and SAR intensity from Sentinel-1 data, in Interferometric Wide (IW) Swath mode, for a temperate raised bog where soil moisture was measured in-situ over the same time period. The occurrence of a large fire on the bog in June-July 2019 presents an opportunity also to understand the effects of wildfire and sudden peatland vegetation loss on the InSAR products such as displacement and coherence (i.e., quality of the InSAR phase). We first introduce the studied peatland and present the spatial observations from remote sensing via both multispectral and SAR data. We then analyse the links between in-situ soil moisture data, SAR intensity and InSAR parameters, as well as their variations due to the fire. Our results provide new insights into the level at which radar backscattering occurs in a temperate raised peatland and into the impacts of wildfire on InSAR in such a setting. Furthermore, these results highlight key elements for time-series InSAR computation on peatlands to maximise the overall coherence (i.e. quality) of the InSAR stack, which will improve the wider application of this remote sensing method to the study of peatlands.

2. Background

2.1. Study site

Ballynafagh bog is a temperate raised peatland located in Ireland (Co. Kildare), (see Figure 1a). Raised peatlands are a wetland type that initiate in waterlogged ground or in enclosed lakes, where decomposition of organic matter is inhibited (Schouten, 2002). With accumulation of organic remains over time, the bog surface rises to several metres above the surrounding land surface and above the regional groundwater table. Raised bogs thus derive water input dominantly or solely from precipitation (i.e. are “ombrotrophic”). As a consequence, they host vegetation adapted to acidic soil conditions and they are highly sensitive to climatic variation. An upper part of the peat (“acrotelm”) is characterised by living plants and aerobic soil conditions, and is typically 0-1 m thick. The lower part of the peat ("catotelm") is characterized by humified plant remains and anaerobic conditions, and is 2-10 m thick.

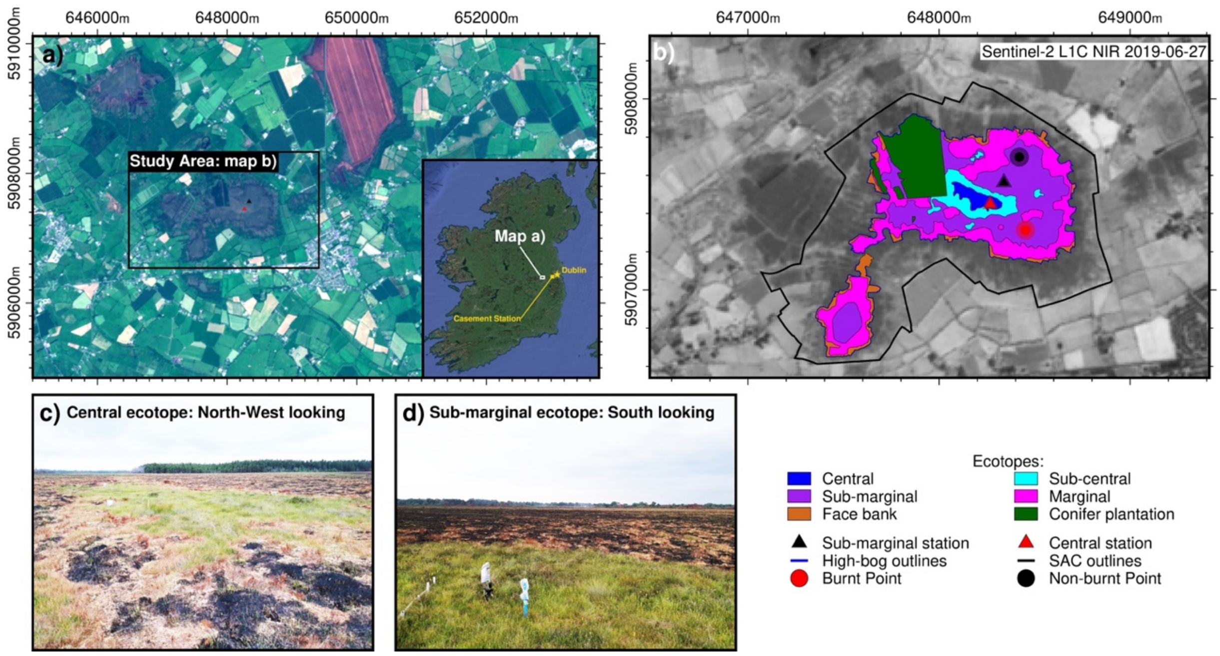

*Figure 1: Ballynafagh bog. **a)** The study area and its surroundings in a Sentinel-2 L1C False Colour image acquired on 2019-06-27, a few days before the wildfire. The inset shows the location of the study area in Ireland (from Google Earth images). **b)** Ecotopes of Ballynafagh bog with the NIR Sentinel-2 L1C image on 2019-06-27 as background. **c)** Post-fire field image, taken on 2019-07-19, of the area around the Central monitoring station. **d)** A post-fire field image, taken on 2019-07-19, of the Sub-marginal monitoring station. Coordinates in meters for UTM zone 29U. The sizes of the point symbols are calibrated to have a radius of 25 m (opaque) and 50 m (clear).*

Ballynafagh bog occurs at the eastern limit of the range of raised bogs in Ireland (Cross, 1990) at an average elevation of 85 m (a.s.l.). The bog is a Special Area of Conservation (SAC), as defined by the European Union's Habitats Directive (Council Directive 92/43/EEC of 21 May 1922). Nearly half the original bog extent within the SAC has been subject to cutting and harvesting of peat in historical times. The harvested area ('cutover area') comprises 90 ha, whereas the uncut area ('high bog') comprises 70 ha. Large drains were installed across the bog throughout the past century for both manual and mechanical peat extraction. In addition, a significant proportion of the bog was damaged by fire during the mid-1990's. Although peat cutting no longer occurs on this site (ceased around 2010), no physical restoration measures have been carried out on site.

Field mapping in 2013, following the classification of Kelly and Schouten (2002), sub-divided the bog surface into several ecotopes (Figure 1b). These are areas of similar vegetation type, ecological condition and microtopography (Fernandez et al., 2014; Kelly & Schouten, 2002). The ecotopes are named Central, Sub-central, Sub-marginal and Marginal, in order of decreasing prevalence of sphagnum mosses and increasing prevalence of heathers and other bushy vegetation. The sphagnum-dominated Central and Sub-central ecotopes represent areas of Active Raised Bog (ARB) (Fernandez et al., 2014), i.e. bog that "still supports significant areas of vegetation which are normally peat forming". These ARB areas, with a net accumulation of peat, covers 6.48 ha (9.25 %) of the uncut (high) bog area, while the remaining 63.58 ha (90.75 %) of the high bog area consists of non-peat accumulating ecotopes. A Pinus Contorta plantation occurs in the North-West of the bog, which occupies 10.02 ha (20 %) of the high bog area and forms a semi-open canopy. The Face Bank ecotope corresponds to the edge of the high bog where recent cutting has occurred and is characterised by a sharp surface gradient from the high bog to the adjacent lower-lying area of cut-over peat.

2.2. Weather and soil conditions time series

Time series of daily and hourly precipitation, soil temperature (to 10 cm depth in mineral soil), potential evapotranspiration and evaporation (Figure 2) are provided by MET Éireann for the Casement station (Lat. 53.303 and Lon. -6.437). This station is twenty kilometres from Ballynafagh bog (Figure 1a). Other meteorological stations are closer to the bog, but these record only daily precipitation and atmospheric temperature, whereas Casement station records data daily, hourly and monitors the full range of soil parameters. Since the temperature and precipitation data from Casement station and from the MET Éireann stations closest to Ballynafagh bog are very similar (see Supplementary Material), we use the Casement data as a proxy for the local meteorological and soil conditions.

Mean annual rainfall from 2017-2021 is 680 mm.yr^{-1}, with a maximum daily precipitation of 45 mm (in winter 2020) and a mean daily rainfall is 2 mm.day^{-1}. Four absolute dry periods (brown bars in Figure 2a) can be defined from daily rain-precipitation measurements: in summer 2018, spring 2020 and summer 2021 (2 periods). Soil temperature is ~10°C on average with a standard deviation of 5°C. and a range from 0°C (measured in 2018) to ~24°C (measured in 2021). Evaporation (Figure 2b) follows the same oscillations in soil temperature. In MET Eireann models, soil moisture deficits reached maxima of ~80-100 mm at the Casement station in summer 2018 and summer 2020.

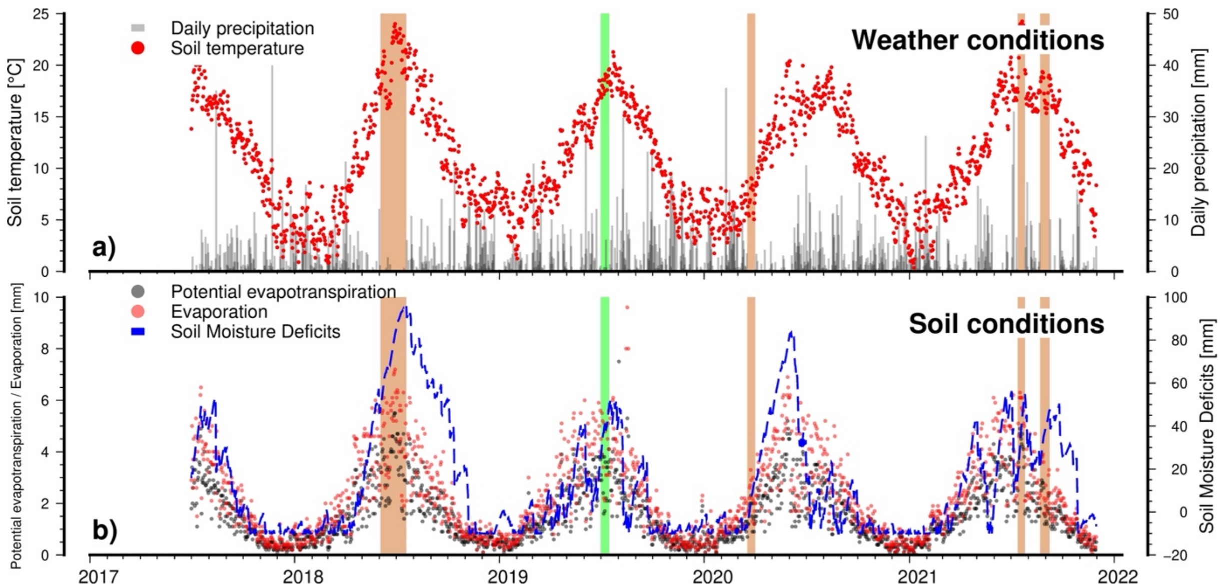

*Figure 2: Time series of weather and soil conditions: **a)** Temporal evolutions of rain precipitation and soil temperature for Casement MET station (Lat. 53.303 and Lon. -6.437) located 22 km from Ballynafagh bog; **d)** Temporal evolutions of potential evapotranspiration, evaporation, and soil moisture deficits (calculated by*

using a 'poorly drained' model) for Casement MET station. The estimated duration of the 2019 wildfire event is displayed as a green bar. Drought periods are indicated by brown bars.

2.3. The 2019 wildfire at Ballynafagh bog

Ballynafagh bog was subjected to a wildfire in July 2019. The start and duration of the fire were not well constrained by local information. A post-fire inspection on the 19th of July 2019 revealed that, where impacted, almost all surface vegetation on the high bog was removed (Figure 1c,d). It was noted, however, that although the bog surface appeared completely scorched, the fire did not appear to affect the peat below 3-5 cm depth. The period of the wildfire in 2019 (green bar in Figure 2) is coincident with the summer peak of temperature and a period of rapidly increasing soils moisture deficits as estimated at the regional Casement MET station. It is worth noting that the summer of 2019 was not the warmest or driest in the period from 2017-2021. Ostensibly, conditions may have been more favourable for wildfires in 2018 and 2020, but ignition did not occur.

3. Methods and Data

3.1. In-situ monitoring data

Two soil moisture monitoring stations were installed in the Central and Sub-marginal ecotopes on the high bog at Ballynafagh in 2017 (Figure 1). The station include METER GS3 sensors, which measure the dielectric permittivity, and by calibration, the soil moisture of the medium in which the sensor is installed. The sensors were planted at 15 cm depth below the peat surface, following excavation of a shallow hole, which was subsequently back filled with the excavated material. Data were logged by using METER EM50 data loggers from 2017 to 2020, and subsequently using METER ZL6 data loggers. The change in data logger type was made to reduce the risk of power loss, as occurred on a few occasions in 2018 and 2019. The ZL6 data loggers are solar powered and, since their installation, data has been continuously monitored every 30 minutes. In March 2019, a piezometer pinned to 1.5 m-depth (with 0.5 m screen) was installed at the Sub-marginal station, where peat thickness is about 8m. The piezometer comprises a 40 mm internal diameter PVC tube, the whole underground section of which is screened, with a HYDROS 21 water level sensor connected to a METER ZL6 data logger. The piezometer continuously logged the water table depth until end of October 2020.

The post-fire inspection on the 19th of July 2019 revealed that the two monitoring stations had escaped any significant damage by the wildfire. The Central station was located at the southern extremity of a c. 20 m by 10 m “island” of preserved or lightly damaged vegetation (Figure 1c). The Sub-marginal station was located within the domain of intact vegetation a few metres from the border of main burn area (Figure 1d). Consequently all sensors continued to function during and after the wildfire.

3.2. Multispectral data processing

To map fire-related vegetation changes at Ballynafagh, we used Sentinel-2 multispectral images at L1C level (without atmospheric correction on radiance measurements) that were acquired before and after the wildfire event. The multispectral bands were cropped and False-Colour, Normalised Difference Vegetation Index (NDVI) and Infrared (IR) images were created (Red: 665 nm, Green: 560 nm, Blue: 490 nm; NDVI: 655 nm and 842 nm; IR: 842 nm, 665 nm, 560). Without changing the coordinate reference system, the spatial resolution of the optical images is 10 metres. From the post-fire NDVI image, we extract the outlines of burnt areas by using segmentation with a minimum threshold of NDVI = 0.2 and a maximum threshold of NDVI = 0.4. Only burnt areas with an area of at least 25 pixels and non-burnt areas of a minimum of 5 pixels (respecting 4-connected pixels) are selected.

3.3. SAR data processing

Synthetic Aperture Radar (SAR) data from the Sentinel-1 satellite mission were used to map changes related to the wildfire also. In addition, InSAR processing of these data were used also to map surface displacements at Ballynafagh bog for the 2017-2021 study period and to examine if the wildfire affected the trends in and/or the quality of InSAR measurements. In the next paragraphs we give a brief overview of the SAR data and InSAR processing to explain the nature, origin and significance of the key parameters analysed later in the study.

During a SAR acquisition, the satellite emits radar waves of a given wavelength that reflect (backscatter) off ground targets. The same satellite then measures the return waves. The result is an image containing a complex number in each pixel in radar geometry – a Single Look Complex (SLC) image. The Sentinel-1 SLC image pixel dimensions are c. 2.3 m range (parallel to the satellite look direction) and c. 13.9 m in azimuth parallel to the satellite flight direction). The modulus of the complex number represents the power of the backscattered signal and is termed the *intensity*. The argument of the complex number is termed the *phase*. The phase is related to: (1) the two-way propagation time of the radar waves between the satellite and the ground; (2) the geometry of acquisition; and (3) the dielectric properties of the ground targets.

The phase information within a single image is not usable because of spatial randomness of the pixel phase, but the difference of phases within two SAR images of the same target area can be calculated to obtain the changes in propagation time. In this case, the phase difference is directly linked to any ground surface displacement that occurred between the two image acquisition dates, as well as to other contributions from topography, satellite orbits, changes in atmospheric conditions, noise, etc. The image obtained by phase differencing is called an interferogram. The stability (i.e. similarity) of the pixel phases between the two SAR acquisitions is termed the coherence (Zebker & Villasenor, 1992). Loss of coherence can be called decorrelation.

The InSAR method for calculating surface displacements consists of firstly accurately repositioning the one image with respect to the other image (coregistration), and then subtracting or minimising the contributions of all the other sources of phase variation, especially topography and atmosphere (Massonnet & Feigl, 1998). The resultant image is termed a differential interferogram, and hence the method is commonly termed D-InSAR. To obtain the time series of surface displacements - i.e., the evolution of displacements for consecutive SAR acquisitions - an inversion can be done upon a network of differential interferograms. The interferograms can computed either relative to one reference image (single reference network) or relative to several reference dates (multi-reference network) (e.g., Casu et al., 2006; Ferretti et al., 2001). The time elapsed between the acquisitions of the SAR images used to generate each interferogram is termed the temporal baseline. A good network design usually minimises the temporal baselines to maximise coherence (i.e. minimise temporal decorrelation).

For this study, InSAR coherence and displacement estimations were derived by processing the Sentinel-1 SLC images acquired, in IW mode, in the Ascending pass and in VV polarisation. All 264 available acquisitions between 4th January 2017 and 18th June 2021 (~4.5 years) were used: 130 from S1A and 134 from S1B. The time interval between acquisitions was typically 6 days (250 images) or at maximum 12-days (14 images). Images acquired in March 2018 during a period of light (a few cm) snow cover are included in the dataset, but any effects on the results from snow cover are within noise. The coregistration was performed by using the GAMMA® software and the Shuttle Radar Topography Mission (SRTM) Digital Elevation Model (DEM), (Farr et al., 2007; Scheiber & Moreira, 2000; Wegmüller et al., 2015; Wegnüller et al., 2016).

From our coregistered SLC stack, the conversion of radar phase to displacement was achieved by using the GAMMA® Interferometric Point Target Approach (IPTA) with a multi-reference network of interferograms (Werner et al., 2003). This interferogram network included both single-look and multi-look images. The latter are derived by a kernel-based image averaging of 10 pixels in range and 2 pixels in azimuth (i.e. a 10/2 multi-look factor) to increase signal-to-noise ratio at the lower spatial resolution. The interferogram network for displacement estimation was created as follows: if N is the index of a SAR acquisition, all N-1, N-2, N-3 interferograms are used together with the N-3 months and N-1 year interferograms, (see Supplementary material) (Ansari et al., 2021; Thollard et al., 2021).

The target points were selected in the following steps and with the following criteria. Firstly, single-look points were selected based on phase stability (i.e., coherence) and amplitude deviation (from the mean) (Werner et al., 2003). Secondly, these single-look points were merged with all multi-looked point data inside the same data stack. Thirdly, the phase of the merged data stack is modelled for unwrapping, under the assumption that the contributions from atmosphere and topography greatly exceed those due to displacement, i.e.:

$$\varphi_{obs} = h \times B_{\perp} + a \tag{1}$$

, where, (for each interferogram), φ_{obs} is the observed phase, h is the SAR geometry constant, $B_{\perp}$ is the perpendicular baseline of the interferogram and a is the residual phase (interpreted as atmosphere). Where a point displays a phase uncertainty value with respect to the modelled value of greater than 1.3 radians, it is removed from the stack. This uncertainty threshold value is based on trial and error; increasing this threshold, we can select more points/pixels but with lower confidence. The key parameters and values used in the IPTA processing are listed in Table S1 (see Supplementary material).

In parallel, coherence maps were computed by using a 10/2 multi-look (as for the IPTA processing) and a 5 x 5 pixel estimation kernel (in radar geometry). Geocoding of images was done with a spatial resolution compatible with the SAR resolution (~ 30 x 30 metres). To investigate the variation of coherence around the two in-situ monitoring stations, we used the same estimation parameters, regarding the multi-look kernel and kernel for estimating the coherence, and the coherence was filtered by using a mean kernel of 3 x 3 pixels, centred on the pixels containing each station. Thus, the coherence around each in-situ stations represents an average value for a range/azimuth area of dimension ~ 150 x 150 m.

4. Results

4.1. RGB and NDVI mapping of the wildfire-affected areas

Sentinel-2 L1C False Colour images with minimal cloud coverage (and similar colour dynamics) show that the burnt areas in the central part of the bog are identifiable by lighter colours in the post-fire image (Figure 3 a-b). By comparing these maps with Figure 1b-c, we can also see that the Central station is surrounded (preserved on its "island") by burning and that the Sub-marginal station is located at the edge of the burnt area. The NDVI images (c.f., Figure 3 c-d) allow a more precise delimitation of the burnt areas: the NDVI there decreases from a pre-fire value of $0.53 \pm 0.03 (1\sigma)$ to a post-fire value of $0.33 \pm 0.04 (1\sigma)$. In other areas that from field inspection were demonstrably unaffected by the fire, such as the northern part of the high bog (NDVI > 0.5), little or no change in NDVI occurs between the pre-fire and post-fire images. The red contours on Figure 3d represent the boundaries of areas affected by the fire as derived from the threshold of NDVI change. These contours collectively encompass an area of 0.47 km^2, which means that about 60-70 % of the high bog area has been affected and damaged by the wildfire.

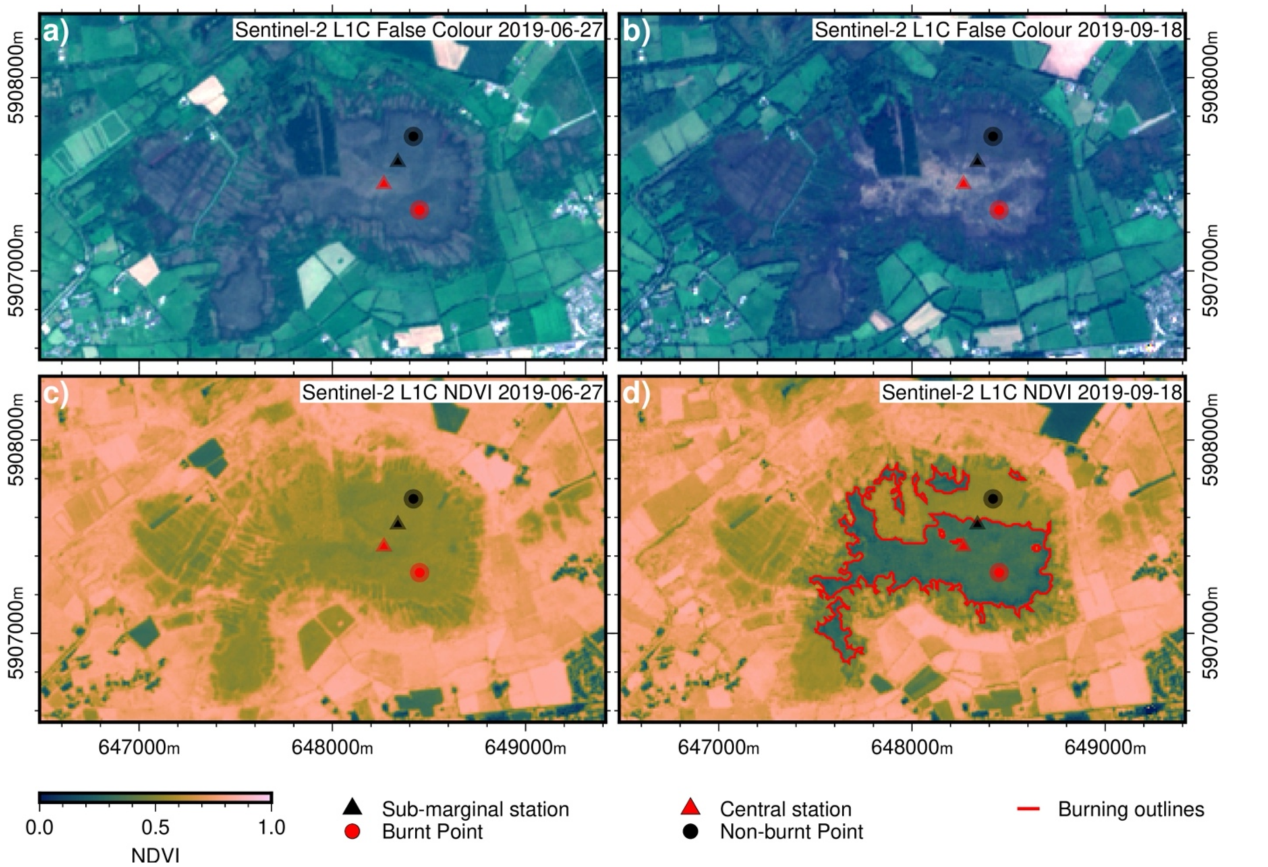

Figure 3: Maps of optical remote sensing data for Ballynafagh bog. ***a)-b)*** *Sentinel-2 L1C false colour images acquired before (on 2019-06-27) and after (on 2019-09-18) the wildfire in July 2019. Spectral bands are Red: 665 nm, Green: 560 nm, Blue: 490 nm;* ***c)-d)*** *NDVI from Sentinel-2 L1C images acquired on 2019-06-27 and 2019-09-18 (655 nm and 842 nm), with the outline of burnt areas in red. Coordinates are in meters for UTM zone 29U. The sizes of the point symbols are calibrated to have a radius of 25 m (opaque) and 50 m (clear).*

4.2. SAR backscatter intensity maps and wildfire duration

SAR backscatter intensity maps also enable delimitation of the wildfire and estimation of its duration. Figure 4 shows the maps of mean SAR backscatter intensity in VV polarisation acquired over Ballynafagh bog for the pre-fire and post-fire periods. On the pre-fire map (Figure 4a), the bog is characterised by a relatively low SAR backscatter intensity (~ -11 dB) with low spatial variation (i.e., -13 dB to -10 dB). On the post-fire map (Figure 4b), the burnt areas of the bog are visible as areas of increased average intensity of ~ -9 dB. This post-fire increase in SAR intensity of 2-3 dB (Figure 4c) delineates the fire extent and is consistent with the fire-affected areas as extracted by the NDVI images (Figure 3). No fire-related variation was observed with the VH polarisation (see Supplementary Materials).

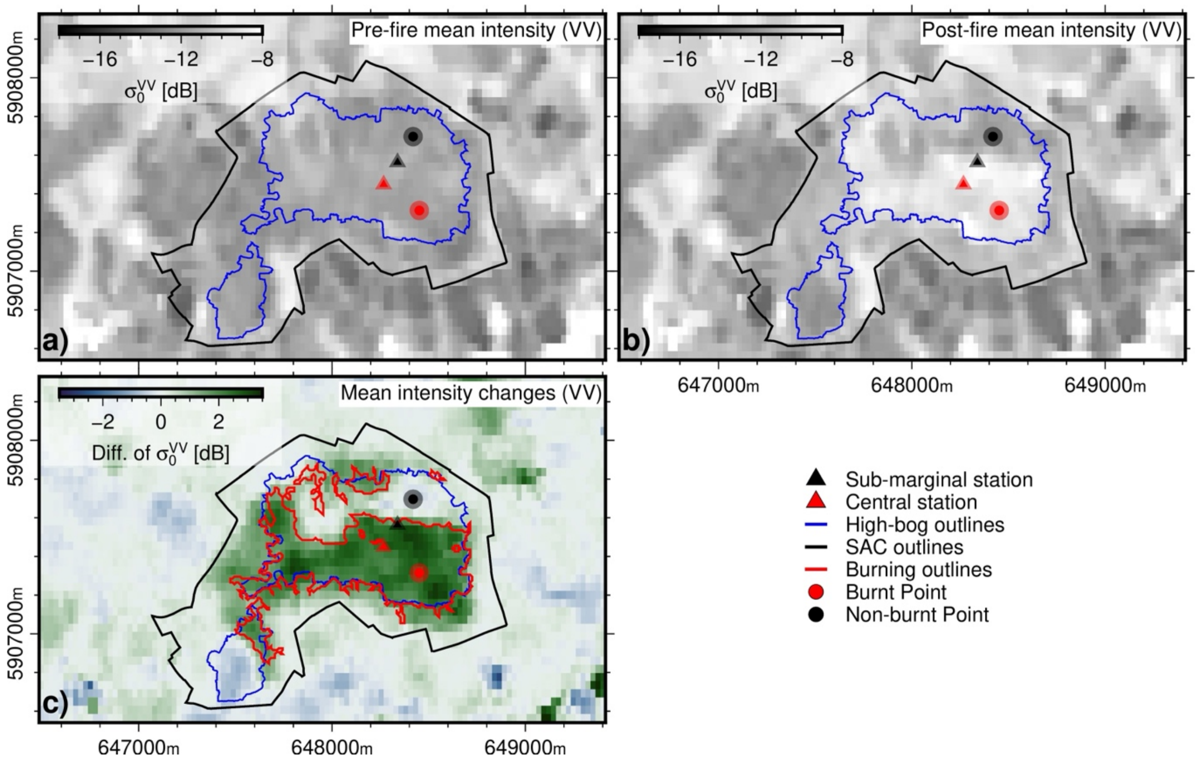

Figure 4: SAR backscatter intensity maps. ***a)*** *Pre-fire mean VV intensity.* ***b)*** *Post-fire mean VV intensity.* ***c)*** *Difference of mean VV intensities: i.e., pre-fire minus post-fire. The sizes of the point symbols are calibrated to have a radius of 25 m (opaque) and 50 m (clear).*

Since SAR waves penetrate clouds, backscatter maps complement the use of multispectral images in constraining the start and end dates of the wildfire. From the combination of Sentinel-2 RGB, IR and NDVI images and Sentinel-1 VV-VH images (see Supplementary Materials), we estimate that the wildfire began after 1st July 2019 and reached its final extent by 5th July 2019. Field observations confirm that the wildfire had stopped burning sometime before 19th July 2019.

4.3. Time series of SAR backscatter intensity and in-situ soil parameters

Figure 5 presents the time-series of SAR backscatter intensity at the Sub-marginal (Figure 5a) and Central (Figure 5b) monitoring stations. Since areas immediately around the monitoring stations have undergone partial burning, we also show data in Figure 5c for two areas located further inside the burnt and non-burnt areas of the peatland (red and black points, respectively, in Figure 4) – both within the same ecotope (sub-marginal). The SAR backscatter intensities (σ_0) at the Sub-marginal and Central stations show a similar temporal evolution. As on the maps in Figure 4, the mean SAR backscatter intensity increases after the wildfire fire by 2-3 dB at both stations and in the wider burnt area. This step-like increase in intensity is not observed in the non-burnt area (Figure 5c). In addition the annual SAR intensity fluctuations could be higher for burnt areas compared to non-burnt areas but the descripted time series of SAR intensity contain a single post-fire oscillations. Qualitatively, it seems that the minimal peak of SAR intensity (in summer 2020) remains equal for the burnt and non-burnt areas.

The SAR backscatter intensity is also affected by annual oscillations of soil moisture and groundwater level (Figure 5). Soil moisture is highest – typically at saturation (or at sensor detection limit) – during the winter and early spring months. Soil moisture decreases to its lowest values during the summer months. Average groundwater level at the Sub-marginal station is 8 cm below the ground surface (see Figure 5a). In winter, the groundwater levels reach up 4 cm below the ground surface, and declines up to 32 cm in summer. Groundwater and soil moisture changes are positively correlated in time.

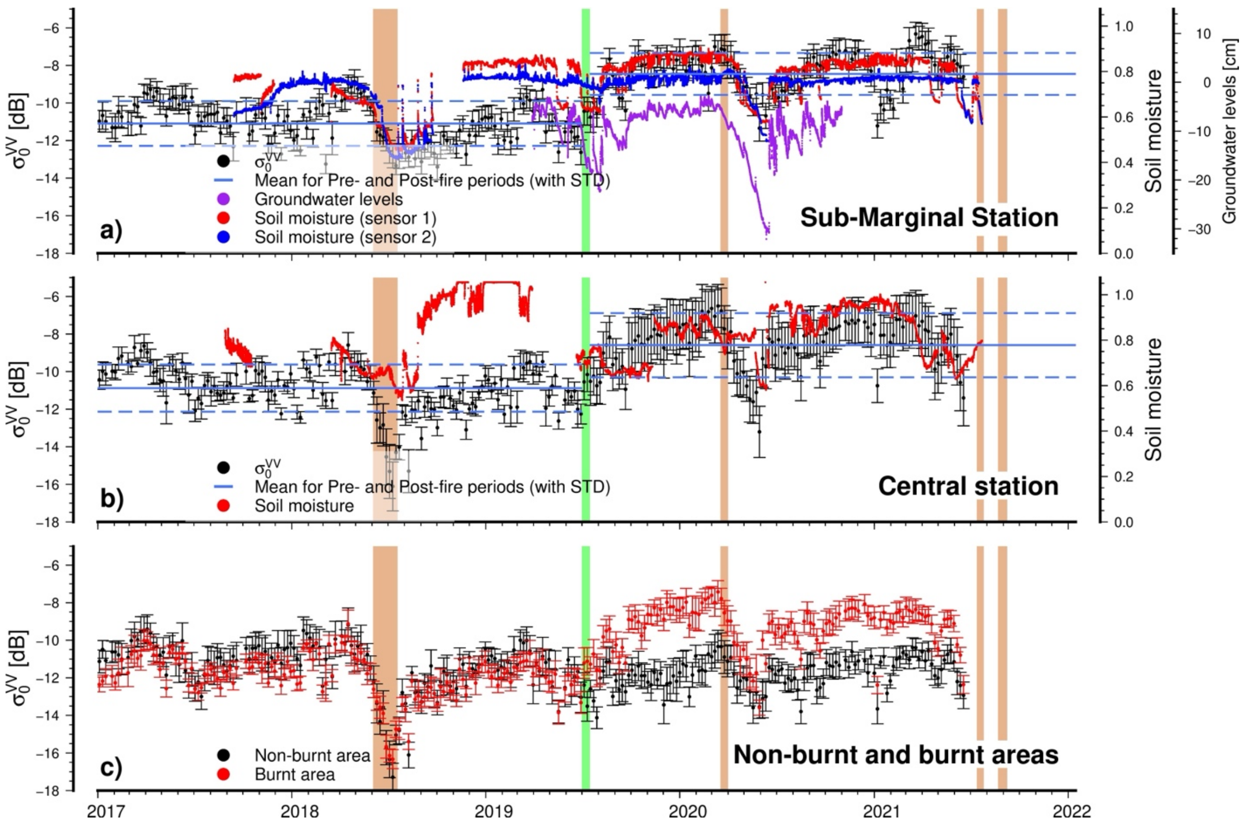

Figure 5: Time series of SAR backscatter intensity. ***a)-b)*** *Temporal evolution of SAR backscatter intensity in VV polarisation at the Sub-marginal station (in* ***a)****) and at the Central station (in* ***b)****).* ***c)*** *Temporal evolution of SAR backscatter intensity in VV polarisation for burnt and non-burnt areas. The estimated duration of the 2019 wildfire event is displayed as a green bar. Drought periods are indicated by brown bars.*

Table 1 gives the Pearson's correlation coefficient (r) between SAR intensity and soil moisture. These parameters are well-correlated (r > 0.5) at the Sub-marginal station, but poorly correlated at the Central station (r < 0.2). However, the intensity at Central station correlates well with soil moisture measured at the Sub-marginal station (r=0.76) meaning that the poor correlation is likely a local effect and caused by the temporal evolution of soil moisture at the Central station.

Table 1: Table of Pearson's correlation coefficient (r) between soil moisture (SM), and SAR backscatter intensity (VV polarisation) for the different soil moisture sensors.

	Soil Moisture		
	Sub-Marginal sensor 1:	**Sub-Marginal sensor 2:**	**Central sensor:**
Intensity Local	0.57 (p_value<0.001)	0.54 (p_value<0.001)	0.19 (p_value=0.004)
Intensity Burnt area	0.56 (p_value<0.001)	0.52 (p_value<0.001)	0.19 (p_value=0.004)
Intensity Non-burnt area	0.70 (p_value<0.001)	0.61 (p_value<0.001)	0.17 (p_value=0.013)
Intensity at Central	0.76 (p_value<0.001)	-	-

The corresponding time series of SAR backscatter intensity are given in Supplementary Materials for the VH polarisation. Overall, the VH times series are noisier than the VV results and are also correlated with soil moisture, but there is not increase in SAR intensity after the wildfire. The SAR data in VH polarisation are therefore not affected by the wildfire.

4.4. Peatland surface motion mapped with InSAR

Figure 6 shows the estimated linear velocity of peatland surface motion over the 4.5-year observation period. Each coloured point corresponds to a pixel that displays suitably high coherence and low phase uncertainty throughout the observation period. Overall, point coverage is good across the high bog area, especially in the sphagnum-dominated or sphagnum-rich ecotopes (Central, Sub-central and Sub-marginal). Point retrieval is more challenging in the areas of marginal ecotope, face bank and the cut-over peat.

We report the Line of Sight (LOS) displacements in our study, with negative values meaning motion away from the satellite and positive values meaning motion toward the satellite. Based on the expected vertical motions for this target, and a conversion factor of 1.3 (i.e., cosine of incidence angle), we can interpret the LOS displacement as vertical displacement, such that a negative value implies subsidence, and a positive value implies uplift. In general, we consider an absolute LOS velocity of more than 1 $mm.yr^{-1}$ to be significant (Fiaschi et al., 2019).

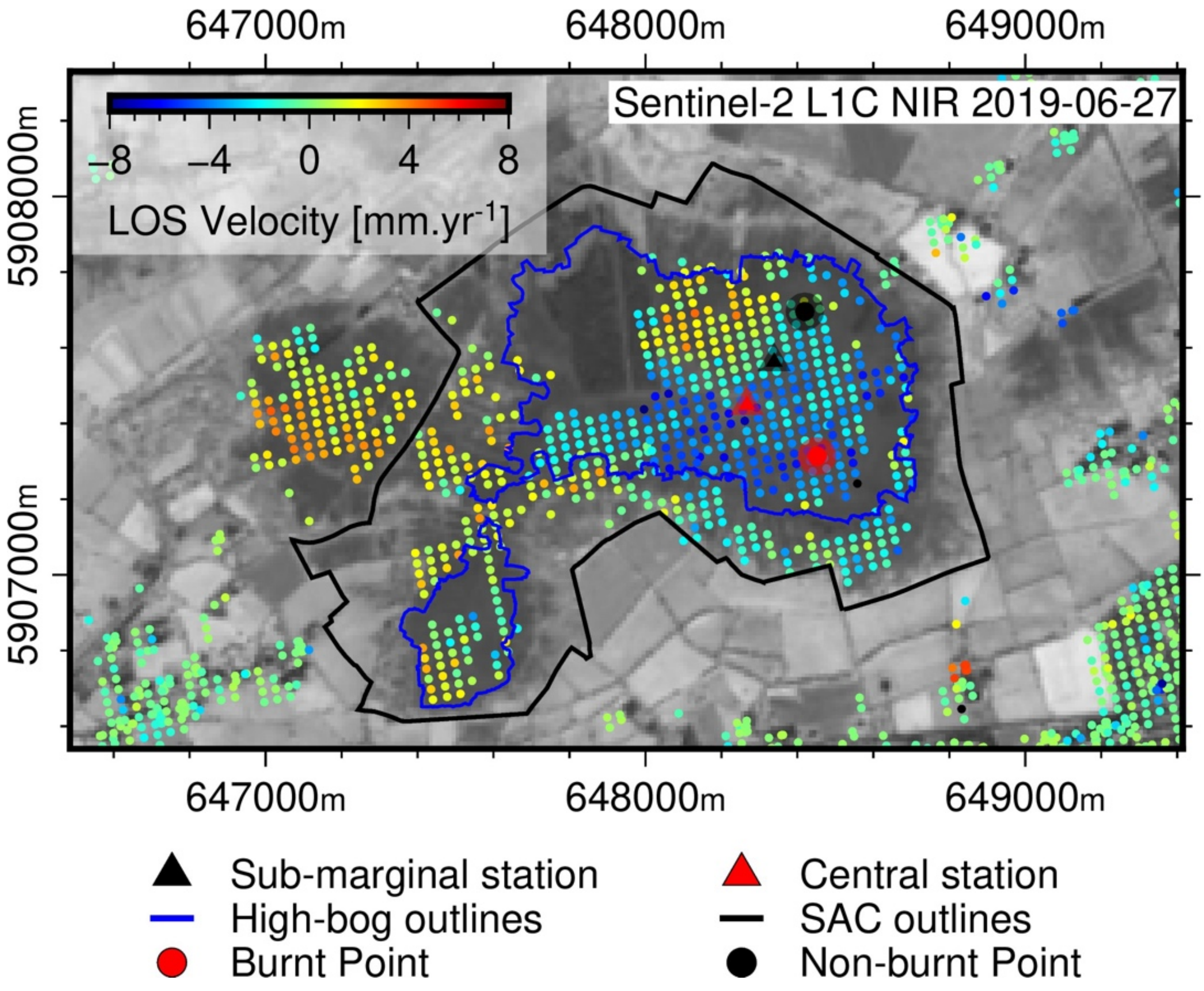

Figure 6: InSAR estimate of peatland surface displacements rates in satellite LOS for the period 2017-2021 with NIR Sentinel-2 L1C image on 2019-06-27 as background. Coordinates are in meters for UTM zone 29U. The sizes of the point symbols are calibrated to have a radius of 25 m (opaque) and 50 m (clear).

The InSAR velocity data indicate that during the observation period most of the high bog area, straddling the Central, Sub-central, and Sub-marginal ecotopes, has undergone subsidence at average vertical rates of up to -9 $mm.yr^{-1}$ (LOS rates of -6.9 $mm.yr^{-1}$). Several other areas within and just outside the SAC boundary are apparently affected by uplift at average vertical rates of up to +5 $mm.yr^{-1}$ (LOS rates of +3.8 $mm.yr^{-1}$). These areas include a northern part of the high bog classified mainly as Marginal ecotope, as well as zones of cut-over (i.e., harvested) bog to the west. The obtained InSAR-derived velocities are thus dichotomous and somewhat heterogenous, but they overall display a broad consistency in space across the bog.

4.5. Time-series of InSAR-derived displacements and in-situ soil parameters

The time series of peat surface displacements around the Sub-marginal, Central in-situ monitoring stations, burnt and non-burnt points (average radius of 25 m; four, two, one and two target points respectively) show long-term linear LOS displacement trends, of $-1.5\pm0.2(1\sigma)$ $mm.yr^{-1}$, $-3.7\pm0.2(1\sigma)$ $mm.yr^{-1}$, $-2.5\pm0.2(1\sigma)$ $mm.yr^{-1}$ and $-0.4\pm0.2(1\sigma)$ $mm.yr^{-1}$, respectively (Figure 7). Superimposed on these long-term trends are roughly annual oscillations in surface displacement of up to ±10 mm. Maximum uplift typically occurs between January-March (winter), whereas maximum subsidence typically occurs in June-August (summer).

395 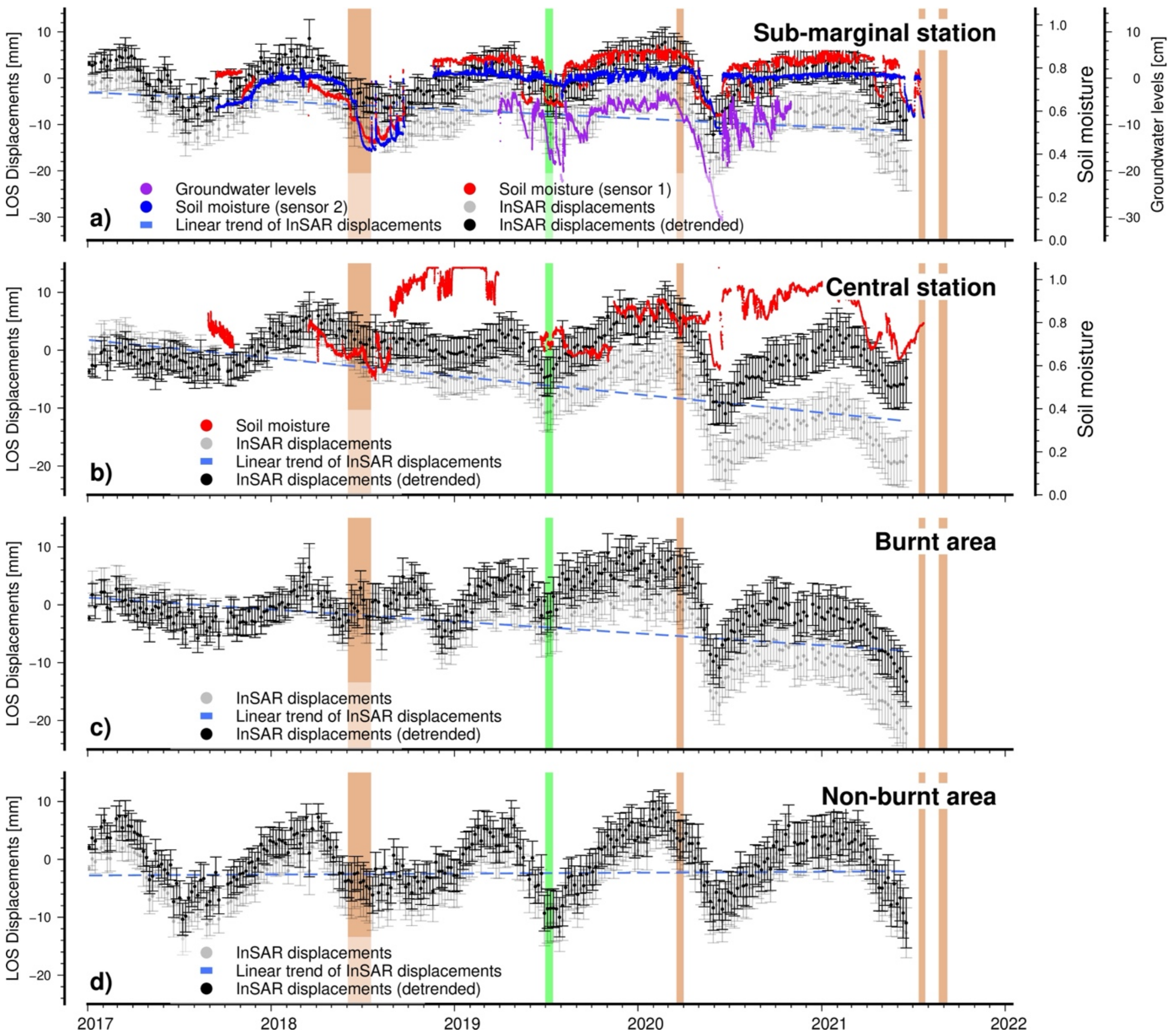

Figure 7: Time series of in-situ measurements and InSAR-derived displacements. ***a)-b)*** *Temporal evolutions of LOS displacements, soil moisture for the Sub-marginal station (in* ***a)****) and for the Central station (in* ***b)****), with the groundwater levels.* ***c)-d)*** *Temporal evolutions of LOS displacements for the burnt area (in* ***c)****) and for the non-burnt area (in* ***d)****). The estimated duration of the 2019 wildfire event is displayed as a green bar. Drought periods are indicated by brown bars.*

The temporal evolution InSAR-estimated surface displacement at Ballynafagh bog tracks the temporal evolution of soil moisture and groundwater levels measured in-situ (Figure 7a-b). The oscillations in the InSAR-derived displacements are near synchronous with both groundwater and soil moisture variations. For the sub-marginal station, soil moisture data is positively and significantly correlated (*p*_value < 0.001) with detrended InSAR displacement (see Table 2). The Pearson's coefficient for linear regression (r), between soil moisture and InSAR-derived displacement is 0.69 for sensor 1 and 0.54 for sensor 2. For the Central station, the soil moisture is poorly correlated with InSAR displacement immediately around that station. However, the soil moisture data at the Central station are positively and significantly correlated with the InSAR displacement at the submarginal station (see Table 2). Although the timescale of seasonal soil moisture and groundwater level decreases is similar to the timescale of seasonal subsidence estimated from InSAR, the recovery of soil moisture and groundwater to high levels may be much sharper for some oscillations (e.g., 2020) – i.e. occurs over a much shorter timescale – than the seasonal upswing in surface displacement. Finally, the magnitudes of changes in groundwater and ground surface levels are in ratio of roughly 10:1.

Table 2: Table of Pearson's correlation coefficient (r) between soil moisture (SM), detrended InSAR displacement for the different soil moisture sensors.

	Soil moisture		
	Sub-Marginal sensor 1:	**Sub-Marginal sensor 2:**	**Central sensor:**
InSAR Local	0.67 (*p*_value<0.001)	0.54 (*p*_value<0.001)	0.05 (*p*_value=0.43)
InSAR Burnt area	0.27 (*p*_value<0.001)	0.19 (*p*_value=0.006)	0.14 (*p*_value=0.038)
InSAR Non-burnt area	0.57 (*p*_value<0.001)	0.44 (*p*_value<0.001)	0.36 (*p*_value<0.001)
InSAR at Central	0.35 (p_value<0.001)	-	-

The InSAR displacement time series for both points located show no clear effect due to the wildfire (Figure 7a-b). The long-term LOS velocities appear to be lower at these points than those observed at the in-situ stations (-2.5±0.2(1σ) mm.yr^{-1} and -0.4±0.2(1σ) mm.yr^{-1} respectively), while the annual oscillations are very similar (Figure 7). The variations in long-term velocity and in the magnitude of annual oscillations further show that the InSAR-derived displacements are dichotomous and heterogenous within the bog. However there is no shift or variation in the burnt area displacement time series that is coincident with the wildfire.

4.6. Evolution of InSAR Coherence

Consistent with the InSAR-derived surface displacement evolution, there is not a systematic pattern of spatial or temporal change in the coherence that one can relate to the wildfire. Figure 8 shows the changes in coherence over Ballynafagh bog in the days before and after the wildfire. Overall, the coherence on the bog is high to moderately high for the relatively short temporal baselines considered here. The maps with lowest coherence are formed when one SAR image of the pair was acquired on a rainy day – for example, the coherence maps spanning June 23rd - July 5th, June 23rd - July11th, July 23rd - August 4th and July 29th - August 4th. Low coherence thus appears to be simultaneous with differences in precipitation, in groundwater levels, and hence differences in soil moisture, between the pair of SAR image acquisitions. Conversely, high coherence is associated with similar precipitation and soil moisture conditions for the SAR acquisition pair.

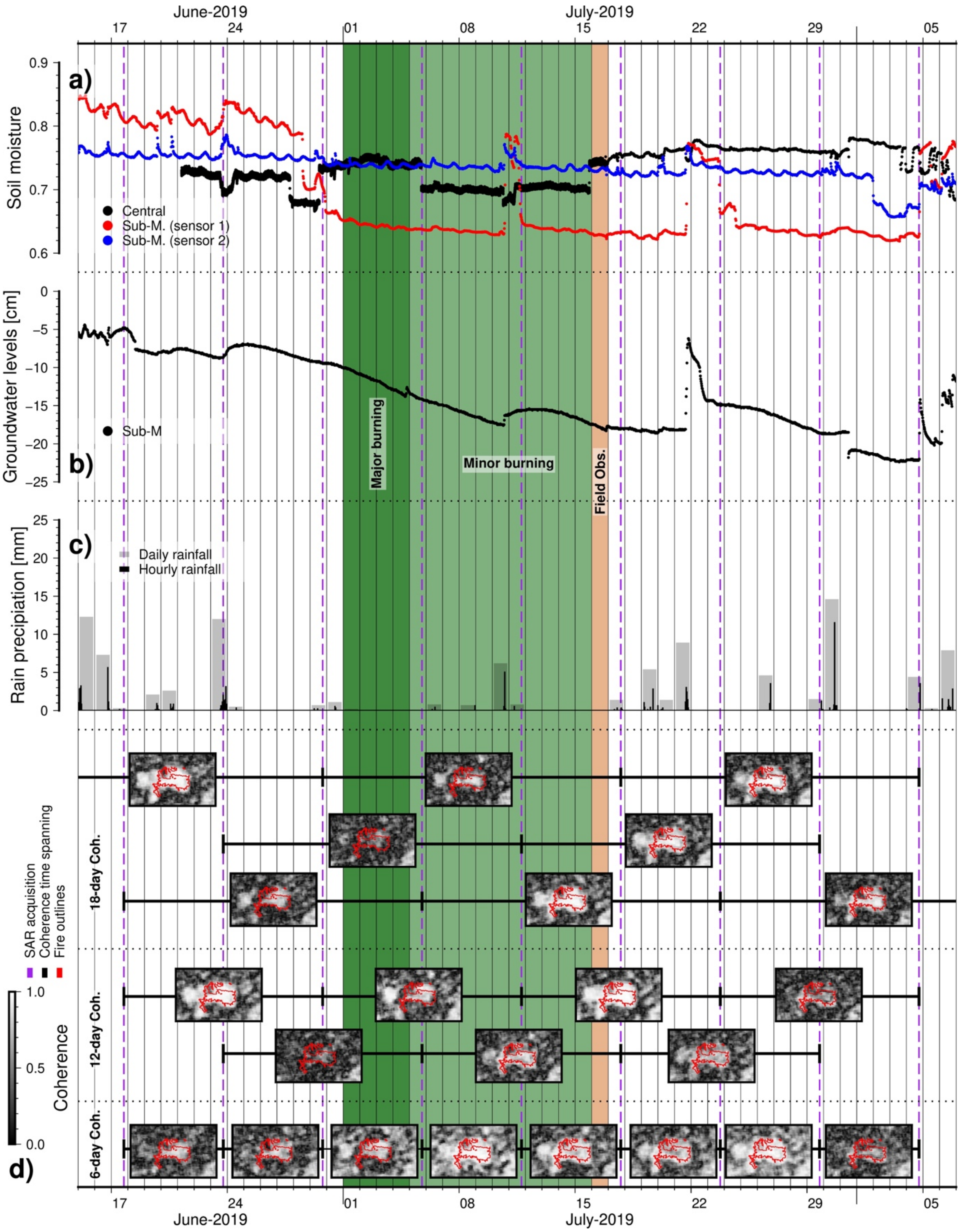

430

Figure 8: Timeline of InSAR coherence maps, weather conditions, soil moisture at Ballynafagh Bog. The upper sections (in ***a)****,* ***b)*** *and* ***c)****) show the temporal evolutions of soil moisture, and groundwater levels as measured*

at Ballynafagh Bog and hourly precipitation as measured at the Casement MET station. The lower section (in ***d)****) shows coherence maps for pairs of SAR images, the acquisition dates of which are given by the bars either side of each coherence map. The rows of coherence maps are arranged from top to bottom in order of decreased temporal baseline. In the greyscale coherence maps, black is low coherence and white is high coherence. The red contour is the outline of the areas affected by the wildfire.*

To illustrate the variation of coherence with soil moisture over the entire observation period, we show a coherence matrix for the areas immediately around both monitoring stations (Figure 9a). Each point in this matrix represents the coherence in each pair of images in the stack at the Central (upper left) or Sub-marginal (lower right) monitoring stations. The image acquisition dates for the pair are given on the horizontal and vertical axes. We make three main observations from the matrix.

Firstly and expectedly, coherence decreases as the temporal baseline of the image pair increases. This is a consequence of temporal decorrelation and is typical of vegetated target areas. This is the main factor controlling coherence on the long term. Secondly, there are abrupt decreases in coherence associated with large differences in soil moisture. These soil moisture-related coherence decreases are superimposed on the background trend of decreased coherence with increased temporal baseline. Coherence loss due to soil moisture difference is particularly pronounced where one SAR image in a pair was acquired during the summers of 2018 or 2020, when large decreases and fluctuations of soil moisture occurred during drought conditions. Under these drought conditions and at short term (< 1 year), high coherence (>0.7) interferograms are formed only from image pairs with a temporal baseline of less than 2-3 weeks. Thirdly and from Figure 9b, the wildfire does not cause a noticeable instantaneous and short-term perturbation on the observed values of coherence compared to the overriding effects of temporal decorrelation and soil moisture difference. The post-burning coherence of the burnt area seems to become slightly higher for longer temporal baselines (>1 year) compared to that of the non-burnt area, but it is unclear if this is a significant change.

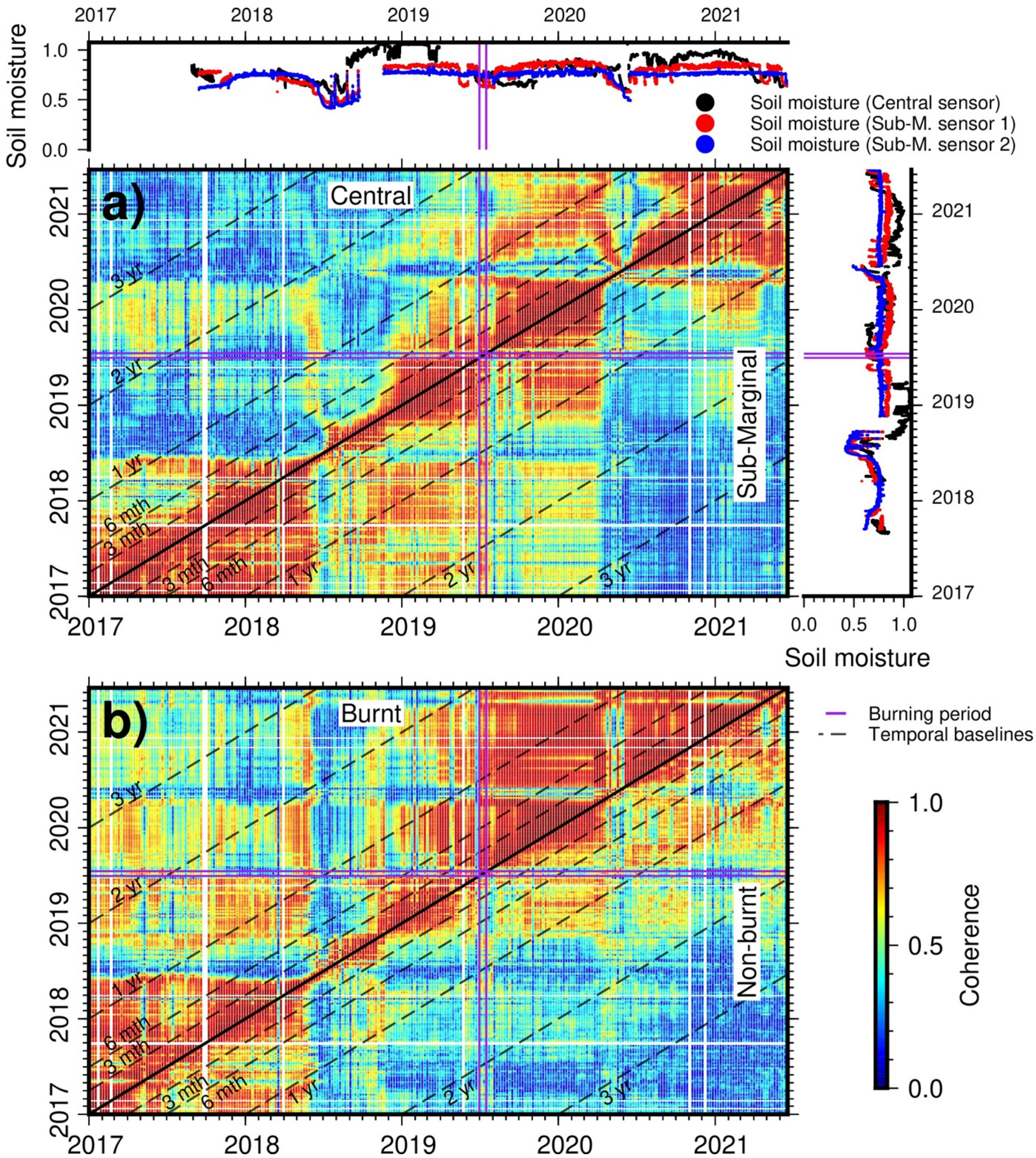

450

Figure 9: Matrix of coherence for all possible SAR image pairs during the observation period ***a)*** *for the in-situ monitoring stations in Ballynafagh bog and* ***b)*** *for the burnt and non-burnt areas as described in Figure 4. For the part* ***a)****, the upper left triangle of the matrix represents coherence values for the area immediately around the station in the Central ecotope. The lower right triangle, on the other side of the solid black diagonal*

*line, represents values for the area around the station in the Sub-marginal ecotope. For the part **b)**, there is a similar layout for the burnt and the non-burnt areas. The matrix plot axes give the acquisition dates of the two SAR images in each pair. The dashed black lines are isochrons that represent where the temporal baselines of image pairs. For comparison to the temporal evolution of the coherence, the temporal evolution of in-situ soil moisture at both stations is displayed on the plots alongside the matrix in part **a)**. The purple lines crossing the matrix and the plots mark the start and end of the wildfire. Overall, as expected, coherence decreases with increased temporal baseline. For a given temporal baseline, however, coherence is higher when soil moisture conditions are similar for each acquisition in an image pair, and coherence is lower when soil moisture conditions differ substantially.*

To examine further the relationship between InSAR coherence, soil moisture change and temporal baseline, we plotted the values of these parameters at the Sub-marginal station (Figure 10). For any value of soil moisture change, a range of coherence can be observed. The maximum value of this coherence range is negatively correlated with soil moisture change – i.e., the greater the soil moisture change, the lower the maximum coherence. Additionally, the coherence is related to the temporal baseline of SAR image pairs. For a given soil moisture change, the coherence is highest for a short temporal baseline and decreases with increased temporal baseline.

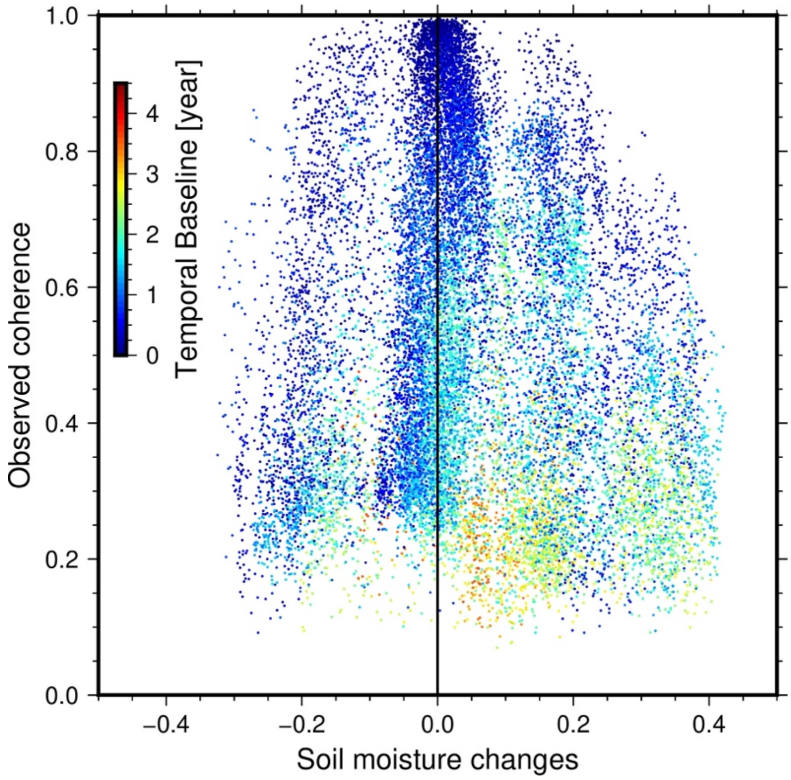

Figure 10: Observed coherence versus soil moisture changes recorded by sensor 1 at the Sub-marginal station. The colour of points gives the temporal baselines of InSAR-coherence images. The two dashed lines represent a schematic maximal value of coherence for a given temporal baselines.

The seasonality of soil moisture changes creates an annual oscillation within InSAR coherence decay in time on the bog. Figure 11 shows the relationship between observed coherence and temporal baseline at the Sub-marginal station, when the first acquisition (reference image) is acquired in a different season. Also plotted for each season is the probability of having a coherence higher than 0.5 for a given temporal baseline. The main trend seen in each graph is the well-known decrease in coherence with increasing temporal baseline. In addition, however, the InSAR coherence oscillates annually. The oscillation of coherence is strongest when the reference image is acquired in the winter, and it is weakest when the reference image is acquired in the summer.

The probability of high coherence (>0.5) is thus linked to the season in which the reference image is acquired. For a reference image acquired in winter, high coherence can be found with temporal baselines of up to three years. For a reference image acquired in summer, on the other hand, high coherence is very unlikely be found with temporal baselines of more than one year.

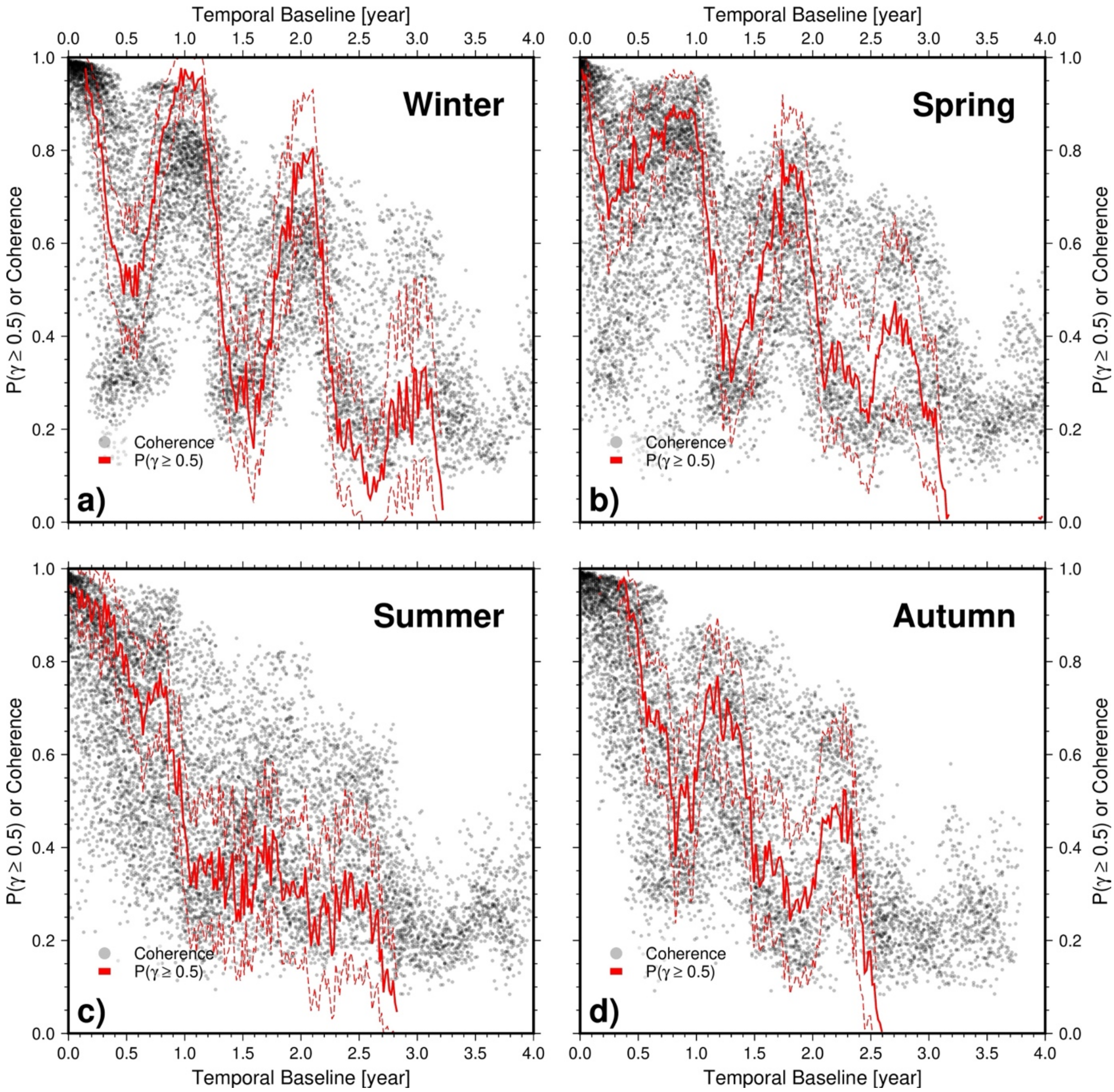

Figure 11: Relationships between the coherence and the probability to have a coherence superior to 0.5 at the Sub-marginal station as a function of temporal baseline, and the season of master acquisition. The dashed lines correspond to 95% confidence levels. The probabilities are estimated using empirical cumulative distribution function (ecdf): $P(\gamma \geq 0.5) = 1 - ecdf(0.5)$.

5. Discussion

The relationships between changes in soil moisture (and vegetation) and SAR intensity, InSAR phase, coherence or closure phase have been well documented in previous works, (e.g., Barrett, 2012; De Zan & Gomba, 2018; De Zan et al., 2014; De Zan et al., 2015; Nesti et al., 1995; Zhang et al., 2008; Zwieback et al., 2015a, 2015b, 2017). However, the continuous monitoring of soil moisture in situ at Ballynafagh bog and the wildfire affecting the bog provide new opportunities to (1) further examine how soil moisture relates to radar remote sensing data at raised peatlands; (2) identify the physical meaning of the SAR/InSAR estimates on peatlands; and (3) improve InSAR processing for retrieval of peatland surface displacement.

5.1. Link between SAR backscatter intensity, soil moisture and groundwater level

SAR backscatter intensity at Ballynafagh bog shows a seasonal variation that closely tracks the meteorological data and soil condition estimates at the regional Casement MET station (Figure 2) and the in-situ parameters at the bog itself (Figure 5). This is true of both VV and VH polarisations (see Supplementary material). The backscatter intensity is reduced as the water table falls and soil moisture is reduced - especially in the periods of drought and or high evaporation in Summer 2018 and Summer 2020 (Figure 2 and Figure 5). This is consistent with previous work that demonstrated a strong positive correlation backscatter intensity with soil moisture in forested areas (Dobson et al., 1992) and with groundwater level in peatlands (Kim et al., 2017). The increase in SAR backscatter intensity at Ballynafagh bog and other sites can be linked to an increase in the dielectric permittivity of the peat as the soil moisture increases (Ayalew et al., 2007; Millard & Richardson, 2018).

5.2. Link between InSAR-derived displacements, soil moisture and groundwater level

In the absence of human interference, the peat-condition at raised bogs is controlled mainly by short-term seasonal and long-term climatic variations (temperature, rainfall and insolation), which control evapotranspiration, soil moisture and water table levels (Heikurainen et al., 1964). Groundwater levels are in turn the main driving force of peat surface displacement (Evans et al., 2021; Hooijer et al., 2010). Indeed surface displacements, in-situ soil moisture, and water table level at Ballynafagh bog all follow similar temporal fluctuations, with an annual periodicity resulting from dry (spring-summer) and wet (autumn-winter) periods.

The short-term (i.e., annual) oscillations in surface displacement at Ballynafagh bog (Figure 7) are consistent with annual variations of surface elevation that are commonly measured in-situ on raised peatlands elsewhere (Evans et al., 2021; Fritz et al., 2008; Howie & Hebda, 2018; Reeve et al., 2013). These annual variations of the peatland surface elevation are termed bog or mire 'breathing', and they are controlled by an annual rise and fall in groundwater levels. The longer-term (multi-annual) displacement trends of subsidence at Ballynafagh bog (Figure 6) could be related to internal peat processes, such as peat compaction and/or oxidation arising from drainage of the bog (Hooijer et al. (2010), and potentially to long-term variations in deeper hydrogeological conditions within or under the peatland, (Ewing & Vepraskas, 2006; Regan et al., 2019).

The correlations at Ballynafagh bog between in-situ soil moisture and peat surface displacement (within 25 m of the in-situ sensors) are strongest for the Sub-Marginal station (Table 2). On the other hand, the correlation between the same parameters is poor at the Central station. However, the soil moisture data from the Central station show a moderate correlation ($r = 0.35$) with InSAR displacement at the sub-marginal station and elsewhere on the bog. From visual inspection of the Central station time-series (Figure 7b), it is apparent that correlation at the station itself is lost firstly in the second half of 2018 and secondly in the second half of 2020. These periods follow very dry summers with drought conditions of up to several weeks in length as represented by: (1) the large falls in soil moisture and groundwater levels locally at Ballynafagh bog (Figure 2a-b); (2) the periods of high temperature and low rainfall regionally (Figure 2a) and (3) the high soil moisture deficits regionally (Figure 2b). Furthermore, the relative recovery of soil moisture following the drought periods is much greater and more rapid at the Central station than at the Sub-marginal station.

Consequently, we suggest that a rapid change in hydrogeological conditions around the Central station following the end of the drought periods in 2018 and 2020 led to an underestimation of the true ground displacement there, and hence a locally poor correlation between soil moisture and InSAR displacement. This is because if rapid change in soil moisture is linked with large and rapid ground displacement, then phase ambiguity may occur such that InSAR underestimates the true displacement of the peat surface (Marshall et al., 2022; Tampuu, 2022). Additionally, as demonstrated here (Figure 11), large soil moisture change can reduce InSAR coherence such that interferograms spanning the period of rapid change are inaccurate.

5.5. The 2019 wildfire and implications for C-band radar penetration and backscattering at raised peatlands

A striking result of our study if Ballynafagh bog is that the average SAR backscatter intensity increases in a step-like manner after the 2019 wildfire (see Figure 4 and Figure 5). In contrast, the InSAR coherence and displacement at Ballynafagh shows no clear effect from the 2019 wildfire. The areas of increased SAR intensity after the wildfire correspond closely to the areas of reduced NDVI on the bog (Figure 3), which we attribute to the removal of the mossy vegetation layer by wildfire (Figure 1c-d). In support of this interpretation, we note that outside the SAC area containing the bog, similar reductions of NDVI are seen also in fields within which grass or cereal crops were recently harvested (Figure 3). **Error! Reference source not found.** shows a schematic interpretation to explain these observations, and the general variation of SAR and InSAR data on the raised peatland, in terms of the propagation and backscattering of the C-band radar beams.

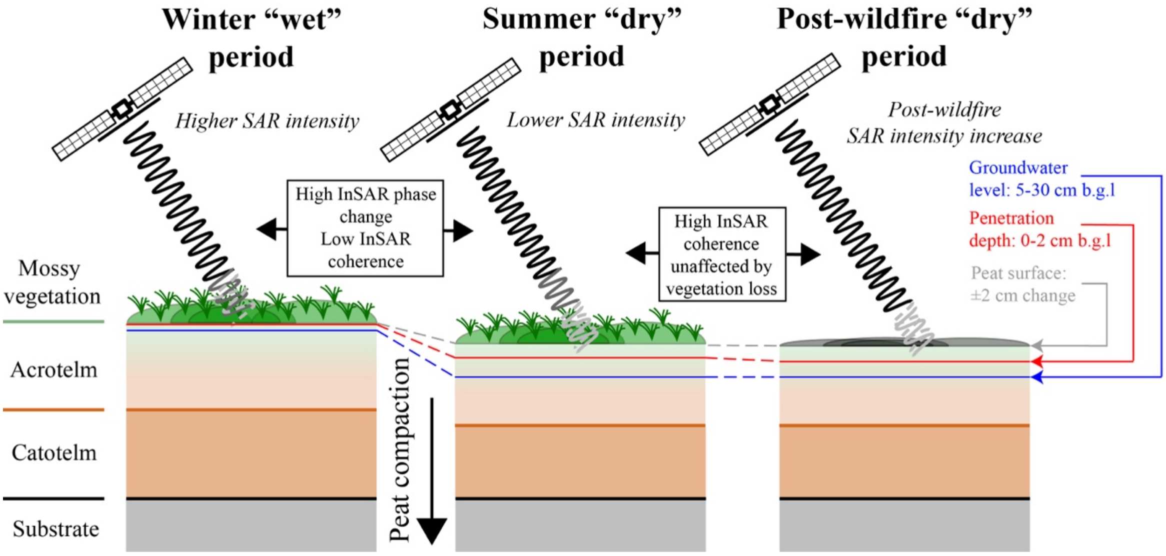

Figure 12: Schematic representation of InSAR propagation in peat associated with climatic controls on soil moisture changes, for active raised bog or healthy areas of bog

During the winter periods, the radar beam propagates though the 10-20 cm thick layer of mossy vegetation and into the upper few mm of the underlying peat. The penetration depth into the peat is likely to be so small, given the high level of groundwater and soil moisture in the wet periods (Nolan and Fatland (2003). Thus most of the radar backscattering occurs at the peat soil surface. The combination of peat and vegetation properties causes attenuation of the SAR backscatter intensity to average values of -10 to -12 dB in VV (see Figure 5) and 9-10 dB in VH (Supplementary material).

During dry summer periods, the radar waves penetrate further into the upper few cm of the peat because the groundwater levels and soil moisture are lower. It is difficult to give an absolute value of the penetration depth into the peat, but given the generally high soil moisture content in peat (a minimum of 0.5 at 15 cm depth during drought – Figure 5 and Figure 7), it is unlikely to be more than a few centimetres (Ayalew et al., 2007; Nolan & Fatland, 2003; Toca et al., 2022). The radar backscatter intensity decreases because of the decreased dielectric permittivity related to the decreased soil moisture content, especially during periods of drought and high temperature. In addition the declining groundwater level leads to subsidence of the peat surface, which is seen as displacement-related phase in InSAR. However, the change in soil moisture between winter and summer periods also decreases InSAR coherence, making accurate detection of such ground displacements more difficult.

After the wildfire, the backscatter intensity for the VV polarisation increases abruptly on average by 2-3 dB, as the attenuation related to 10-20 cm mossy vegetation layer is removed. The SAR backscatter intensity in VH polarisation is not affected by the vegetation removal caused by the wildfire (see Supplementary Materials). Moreover, after the vegetation is removed, the intensity of VV polarised SAR backscatter is the same as the VH polarised backscatter (both average around 9-10 dB). Thus the mossy vegetation structure represents a partial polarised filter attenuating the returning SAR waves in the vertical direction.

Finally, the InSAR phase is unaffected by the vegetation removal due to the wildfire, because the main backscattering level is the peat soil surface. Moreover, if the soil moisture content does not change much between image acquisitions and the severity of the burn is limited, the coherence remains stable and shows no effect from the wildfire.

5.6. Transferability to other peatlands

Our findings are suitable for temperate raised peatlands and further studies should be focused on temperate blanked bog (perhaps temperate fens if the InSAR coherence is enough to produce InSAR time series of displacements). In terms of transferability of these results to other peatlands, we must consider several issues:

1. the extent of raised bogs, as opposed to other peatland types such as blanket bogs and fens. Raised bogs are relatively common in Ireland, making up about 20% of the total current peatland area. In other European countries, however, largely destroyed by human activities;
2. different vegetation and hydrological dynamics at other types of bog. Blanket bog vegetation is similar to that of raised bogs although the hydrological dynamics may differ. Nonetheless InSAR has proven capable to mapping apparent displacement of temperate blanket bogs (Alshammari et al., 2020; Marshall et al., 2022). Fens are characterised by different hydrological dynamics and by more vascular vegetation than raised bogs, with the latter factor making them much more difficult targets for InSAR in our experience;
3. condition of the bog – InSAR works well on relatively intact bogs; in our experience it does not work so well on highly degraded bogs, afforested bogs, or bogs with bare peat.
4. the role of climate: InSAR has apparently worked well to detect displacement at tropical raised bogs (Hoyt et al., 2020). Peatland in boreal or continental climates is likely to be more difficult targets, in part due their being commonly afforested and partly because of long annual periods of snow cover and/or ice which will decrease or destroy coherence and partly because there are much larger changes in temperature and precipitation during the year. For such bogs, such as shown by Tampuu (2022), the underestimation of InSAR-derived displacements during summer is the main challenge for C-band InSAR.

For InSAR coherence, our conclusions on the link between soil moisture changes and coherence-related-moisture value should be transferable to other temperate bogs as we observe minor links between coherence and vegetation types. However, (1) the dielectric constants, which control changes in coherence, may be slight different through peatlands and (2) the temporal decorrelation may vary. Further study could consist of an investigation of these in-situ constants to get a clear picture of the variability of InSAR coherence. Regarding the effects of wildfire, a more intense fire than that at

Ballynafagh in 2019, whereby a significant depth of the peat layer is burned, will likely lead to a loss of coherence as the radar properties of the materials could be modified.

5.3. Implications of soil moisture changes for InSAR computations on peatlands

Another important observation in our study is that the coherence on a raised peatland can increase over time. This partly compensates for typical temporal decorrelation on longer temporal baselines (> 1-2 years), and, to our knowledge, this is only observable on peat targets for these durations. The coherence oscillates with an annual frequency with respect to the first coherence value (Figure 11). Indeed, the coherence remains high several months after the reference acquisition (about 3 months), decreases for durations of about 6 months, then increases 1 year after the first acquisition, and so on (Figure 11). Thus, it is possible to observe medium or high coherence for 1- or even 2-years temporal baselines.

We can define, after simplifications, that:

$$\gamma_{\text{Observed}} = \gamma_{\text{Temporal}} \times \gamma_{\text{Soil Moisture}} \times \gamma_{\text{Noise}}, \qquad (2)$$

with γ the InSAR coherence (Zhang et al., 2008). With a coherence of 0.7 on the 1-2-years interferograms and equation 2, we can interpret that γ_{Temporal} is also higher than 0.7, which demonstrates that temporal decorrelation is extremely low on peatlands: probably the lowest compared to other vegetation targets (Tampuu, 2022). On Figure 13 and for any observed coherence value, InSAR coherence is a product of the three previous terms. Each coherence component tends to decrease the observed coherence. The most visible trend (in red) is a decrease in coherence over time: i.e., the coherence varies from 0 to 0.5 over 4.5 years. This trend is strictly the temporal decorrelation and is characterised by an irreversible decrease. The second variation is shown by the blue line. This decorrelation is characterised by oscillated decorrelation over time. However, it is not temporal decorrelation because the coherence can increase, if the soil moisture changes are low. Then, the last component is the noise decorrelation represented by the purple segment. In our study case, we show that soil-moisture-related coherence ($\gamma_{\text{Soil Moisture}}$) is the main factor controlling the recovery of coherence on interferograms with long temporal baselines (>1-2 years), (see Figure 11 and Figure 13).

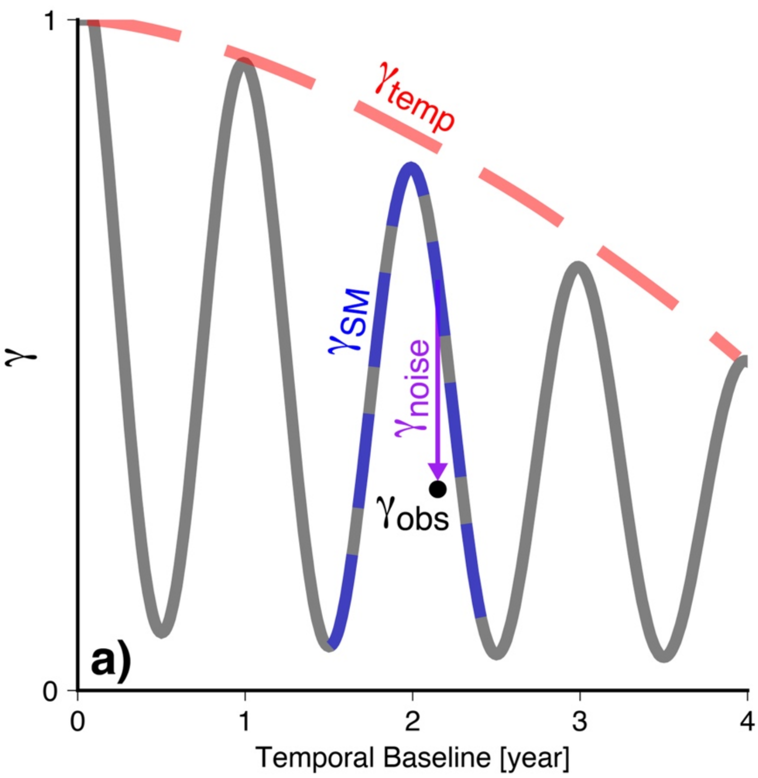

Figure 13: Schematic representation of temporal evolution of InSAR-coherence on Ballynafagh bog. The grey line is the observed InSAR coherence with for components: the temporal coherence in red, the soil-moisture-related coherence in blue and the noise in purple.

Conventional and improved InSAR approaches, suitable for peatland applications, are based on interferogram networks selected to minimise temporal and perpendicular baselines, and hence the coherence of the interferogram stack, (e.g., Alshammari et al., 2020; Alshammari et al., 2018; Bateson et al., 2015; Casu et al., 2006; Cigna, Novellino, et al., 2014; Cigna, Sowter, et al., 2014; Hooper, 2008; Sowter et al., 2013; Werner et al., 2003). Thus, from Figure 11 and Figure 13, the coherence is related to the selection of the reference date on peatlands via soil moisture changes: i.e., it seems more robust to select a reference acquisition (or super single reference regarding the InSAR correlation) in spring in order to maximise the coherence of the whole stack.

According to the proposed InSAR phase and coherence models, the InSAR phase should also be modified by soil moisture (e.g., De Zan et al., 2014; Nolan et al., 2003). However, we are not able to extract this phase due to the peat surface displacements. In addition, we do not observe significative non-zero closure phases in our interferograms for which we have identified changes in soil moisture. This seems expected because the observation of closure phases is defined by our ability to multi-look and filter the SAR/InSAR data, (Eshqi Molan & Lu, 2020b; Molan et al., 2020). In contrast, high residuals of phase are observed during the InSAR processing. These phase residuals map perfectly to the spatial extent of the bog, and they are unrelated to potential atmospheric delay. The InSAR phase in C band that is interpreted as displacement could therefore include part of unobserved soil moisture phase on the peat targets. This could modify the results during the inversion of displacements and cause an underestimation of the amplitudes of the annual oscillations (in the case of peatlands), (Zwieback et al., 2017). This other cause of InSAR-phase modifications may be a potential explanation for the deviations observed in 2018 and 2020 for the Central station between soil moisture and peat surface displacement. Consequently, potential estimation of artefacts due to soil moisture change on InSAR-derived displacements should in future be quantified using with in-situ displacement measurements such as Marshall et al. (2022) and Tampuu (2022).

6. Conclusions

In summary, our study explored the full range of InSAR products and their relationships to in-situ soil moisture and groundwater level measurements over a temperate peatland affected by a wildfire. We draw four main conclusions.

Firstly, the InSAR-estimated peat surface displacements display annual oscillations (“bog breathing”) that are synchronous and positively correlated with the seasonal (dry/wet) evolutions of soil moisture and groundwater levels. Thus, peat surface displacements should be an indicator of short-term variations in ecohydrological parameters, such as groundwater levels.

Secondly, SAR intensity positively correlates with absolute values of soil moisture. Thus, SAR intensity oscillates on seasonal timeframes: it increases in wet periods and decreases in dry periods.

Thirdly, InSAR coherence negatively correlates with changes in soil moisture. Consequently, InSAR coherence is low for large soil moisture changes, and is high for small soil moisture changes between two SAR acquisitions. Moreover, the designing of InSAR stack should take into account the relationship to optimise the coherence of the InSAR stack, and avoid coherence loss due to sharp soil moisture changes especially across dry periods.

Fourth, the wildfire highlighted how SAR and InSAR estimates relate to different attributes for raised peatlands: (1) SAR intensity is affected by both changes in soil moisture and vegetation; (2) InSAR coherence is affected by only soil moisture changes. Consequently, SAR and InSAR data from C-band radar sensor reveal information on different levels in the peat column.

These findings can underpin the application and interpretation of radar in monitoring of peatland soil parameters in general and in areas affected by wildfires. Future work should therefore focus on ground validation of InSAR displacements from in-situ measurements in order to verify the accuracy of

InSAR results and to identify the possible magnitude of bias caused by soil moisture on displacement observations.

Data availability

The additional figures can be found in the Supplementary Materials. All the InSAR products and scripts used to analyse the observations are available from the corresponding authors.

CRediT authorship contribution statement

Alexis Hrysiewicz: Conceptualisation, Data computation, Investigation and Analysis, Methodology, Visualisation, Writing – original draft – review and editing. **Eoghan P. Holohan:** Supervision, Project Funding and administration, Conceptualisation, Investigation and Analysis, Methodology, Visualisation, Writing – original draft – review and editing. **Shane Donohue:** Conceptualisation, in-situ data extraction, Investigation and Analysis, Review. **Hugh Cashnan:** In-situ data extraction and Investigation.

Acknowledgments

Firstly we thank the two reviewers who improved the manuscript via their comments and suggestions and Marie Weiss, editor-in-chief of RSE. The authors also thank John Walsh (UCD) for his support in setting up the InSAR lab at UCD and GAMMA staff for technical support. We acknowledge the European Space Agency (ESA) for the Sentinel-1 data and NASA for SRTM DEM. We also thank Wessel et al. (2019) for the developing and availability of GMT6. The authors acknowledge support from Science Foundation Ireland (SFI), University College Dublin (UCD) and the SFI Research Centre In Applied Geosciences hosted by UCD (iCRAG-Phase 2 – Grand Code: 13/RC/2092_P2).

Declaration of Competing Interest

The authors declare no competing interests.

References

Alshammari, L., Boyd, D. S., Sowter, A., Marshall, C., Andersen, R., Gilbert, P., Marsh, S., & Large, D. J. (2020). Use of Surface Motion Characteristics Determined by InSAR to Assess Peatland Condition. *Journal of Geophysical Research: Biogeosciences*, *125*(1), 1-15. https://doi.org/10.1029/2018JG004953

Alshammari, L., Large, D. J., Boyd, D. S., Sowter, A., Anderson, R., Andersen, R., & Marsh, S. (2018). Long-term peatland condition assessment via surface motion monitoring using the ISBAS DInSAR technique over the Flow Country, Scotland. *Remote Sensing*, *10*(7). https://doi.org/10.3390/rs10071103

Ansari, H., De Zan, F., & Parizzi, A. (2021). Study of Systematic Bias in Measuring Surface Deformation With SAR Interferometry. *IEEE Transactions on Geoscience and Remote Sensing*, *59*(2), 1285-1301. https://doi.org/10.1109/tgrs.2020.3003421

Asmuß, T., Bechtold, M., & Tiemeyer, B. (2018). *Towards Monitoring Groundwater Table Depth in Peatlands from Sentinel-1 Radar Data* IGARSS 2018 - 2018 IEEE International Geoscience and Remote Sensing Symposium, Valencia, Spain.

Ayalew, G., Holden, N. M., & Ward, S. M. (2007). Microwave dielectric properties of horticultural peat products. *Mines and Peat*, *2*(May 2014), 1-10.

Balenzano, Mattia, F., Satalino, Pauwels, & Snoeij. (2012). SMOSAR ALGORITHM FOR SOIL MOISTURE RETRIEVAL USING SENTINEL-1 DATA (1) Consiglio Nazionale delle Ricerche (CNR) – Istituto di Studi sui Sistemi Intelligenti per l ' Automazione (ISSIA), Bari , Italy (2) Ghent University – Laboratory of Hydrology a. (1), 1200-1203.

Balenzano, A., Mattia, F., Satalino, G., Lovergine, F. P., Palmisano, D., Peng, J., Marzahn, P., Wegmüller, U., Cartus, O., Dąbrowska-Zielińska, K., Musial, J. P., Davidson, M. W. J., Pauwels, V. R. N., Cosh, M. H., McNairn, H., Johnson, J. T., Walker, J. P., Yueh, S. H., Entekhabi, D., . . . Jackson, T. J. (2021). Sentinel-1 soil moisture at 1 km resolution: a validation study. *Remote Sensing of Environment*, *263*. https://doi.org/10.1016/j.rse.2021.112554

Barrett, B. (2012). The Use of C- and L-Band Repeat-Pass Interferometric SAR Coherence for Soil Moisture Change Detection in Vegetated Areas. *The Open Remote Sensing Journal*, *5*(1), 37-53. https://doi.org/10.2174/1875413901205010037

Bateson, L., Cigna, F., Boon, D., & Sowter, A. (2015). The application of the intermittent SBAS (ISBAS) InSAR method to the South Wales Coalfield, UK. *International Journal of Applied Earth Observation and Geoinformation*, *34*(1), 249-257. https://doi.org/10.1016/j.jag.2014.08.018

Bechtold, M., Schlaffer, S., Tiemeyer, B., & De Lannoy, G. (2018). Inferring Water Table Depth Dynamics from ENVISAT-ASAR C-Band Backscatter over a Range of Peatlands from Deeply-Drained to Natural Conditions. *Remote Sensing*, *10*(4). https://doi.org/10.3390/rs10040536

Casu, F., Manzo, M., & Lanari, R. (2006). A quantitative assessment of the SBAS algorithm performance for surface deformation retrieval from DInSAR data. *Remote Sensing of Environment*, *102*(3-4), 195-210. https://doi.org/10.1016/j.rse.2006.01.023

Cigna, F., Novellino, A., Jordan, C. J., Sowter, A., Ramondini, M., & Calcaterra, D. (2014). Intermittent SBAS (ISBAS) InSAR with COSMO-SkyMed X-band high resolution SAR data for landslide inventory mapping in Piana degli Albanesi (Italy). *SAR Image Analysis, Modeling, and Techniques XIV*, *9243*, 92431B-92431B. https://doi.org/10.1117/12.2067424

Cigna, F., Sowter, A., Jordan, C. J., & Rawlins, B. G. (2014). Intermittent Small Baseline Subset (ISBAS) monitoring of land covers unfavourable for conventional C-band InSAR: proof-of-concept for peatland environments in North Wales, UK. *SAR Image Analysis, Modeling, and Techniques XIV*, *9243*, 924305-924305. https://doi.org/10.1117/12.2067604

Connolly, J., & Holden, N. M. (2009). Mapping peat soils in Ireland: Updating the derived Irish peat map. *Irish Geography*, *42*(3), 343-352. https://doi.org/10.1080/00750770903407989

Connolly, J., Holden, N. M., & Ward, S. M. (2007). Mapping Peatlands in Ireland using a Rule-Based Methodology and Digital Data. *Soil Science Society of America Journal*, *71*(2), 492-499. https://doi.org/10.2136/sssaj2006.0033

Cross, J. (1990). *The raised bogs of Ireland: their ecology, status and conservation*. Stationery Office.

De Zan, F., & Gomba, G. (2018). Vegetation and soil moisture inversion from SAR closure phases: First experiments and results. *Remote Sensing of Environment*, *217*(2017), 562-572. https://doi.org/10.1016/j.rse.2018.08.034

De Zan, F., Parizzi, A., Prats-Iraola, P., & López-Dekker, P. (2014). A SAR interferometric model for soil moisture. *IEEE Transactions on Geoscience and Remote Sensing*, *52*(1), 418-425. https://doi.org/10.1109/TGRS.2013.2241069

De Zan, F., Zonno, M., & Lopez-Dekker, P. (2015). Phase Inconsistencies and Multiple Scattering in SAR Interferometry. *IEEE Transactions on Geoscience and Remote Sensing*, *53*(12), 6608-6616. https://doi.org/10.1109/TGRS.2015.2444431

Dobson, M. C., Pierce, L., Sarabandi, K., Ulaby, F. T., & Sharik, T. (1992). Preliminary analysis of ERS-1 SAR for forest ecosystem studies. *IEEE Transactions on Geoscience and Remote Sensing*, *30*(2), 203-211.

Drösler, M., Freibauer, A., Torben, C. R., & Friborg, T. (2008). Observations and status of peatland greenhouse gas emissions in Europe. In *The Continental-Scale Greenhouse Gas Balance of Europe* (pp. 243--261). Springer. https://doi.org/10.1007/978-0-387-76570-9

Eshqi Molan, Y., & Lu, Z. (2020a). Can InSAR Coherence and Closure Phase Be Used to Estimate Soil Moisture Changes? *Remote Sensing*, *12*(9). https://doi.org/10.3390/rs12091511

Eshqi Molan, Y., & Lu, Z. (2020b). Modeling InSAR Phase and SAR Intensity Changes Induced by Soil Moisture. *IEEE Transactions on Geoscience and Remote Sensing*, *58*(7), 4967-4975. https://doi.org/10.1109/tgrs.2020.2970841

Evans, C. D., Callaghan, N., Jaya, A., Grinham, A., Sjogersten, S., Page, S. E., Harrison, M. E., Kusin, K., Kho, L. K., Ledger, M., Evers, S., Mitchell, Z., Williamson, J., Radbourne, A. D., & Jovani-Sancho, A. J. (2021). A Novel Low-Cost, High-Resolution Camera System for Measuring Peat Subsidence and Water Table Dynamics. *Frontiers in Environmental Science*, *9*. https://doi.org/10.3389/fenvs.2021.630752

Ewing, J. M., & Vepraskas, M. J. (2006). Estimating primary and secondary subsidence in an organic soil 15, 20, and 30 years after drainage. *Wetlands*, *26*(1), 119-130. https://doi.org/10.1672/0277-5212(2006)26[119:EPASSI]2.0.CO;2

Farr, T. G., Rosen, P. A., Caro, E., Crippen, R., Duren, R., Hensley, S., Kobrick, M., Paller, M., Rodriguez, E., Roth, L., Seal, D., Shaffer, S., Shimada, J., Umland, J., Werner, M., Oskin, M., Burbank, D., & Alsdorf, D. E. (2007). The shuttle radar topography mission. *Reviews of Geophysics*, *45*(2), RG2004-RG2004. https://doi.org/10.1029/2005RG000183

Fernandez, F., Connolly, K., Crowley, W., Deneyer, J., Duff, K., & Smith, G. (2014). *Raised Bog Monitoring and Assessment Survey 2013*.

Ferretti, A., Prati, C., & Rocca, F. (2001). Permanent scatterers in SAR interferometry. *IEEE Transactions on Geoscience and Remote Sensing*, *39*(1), 8-20. https://doi.org/10.1109/36.898661

Fiaschi, S., Holohan, E. P., Sheehy, M., & Floris, M. (2019). PS-InSAR Analysis of Sentinel-1 Data for Detecting Ground Motion in Temperate Oceanic Climate Zones: A Case Study in the Republic of Ireland. *Remote Sensing*, *11*(3). https://doi.org/10.3390/rs11030348

Fritz, C., Campbell, D. I., & Schipper, L. A. (2008). Oscillating peat surface levels in a restiad peatland, New Zealand-magnitude and spatiotemporal variability. *Hydrological Processes*, *22*(17), 3264-3274. https://doi.org/10.1002/hyp.6912

Gorham, E. (1991). Northern Peatlands: Role in the Carbon Cycle and Probable Responses to Climatic Warming. *Ecol Appl*, *1*(2), 182-195. https://doi.org/10.2307/1941811

Heikurainen, L., Päivänen, J., & Sarasto, J. (1964). Ground water table and water content in peat soil.

Hiraishi, T., Krug, T., Tanabe, K., Srivastava, N., Baasansuren, J., Fukuda, M., & Troxler, T. (2014). 2013 supplement to the 2006 IPCC guidelines for national greenhouse gas inventories: Wetlands. *IPCC, Switzerland*.

Hooijer, A., Page, S., Canadell, J. G., Silvius, M., Kwadijk, J., Wösten, H., & Jauhiainen, J. (2010). Current and future CO 2 emissions from drained peatlands in Southeast Asia. *Biogeosciences*, *7*(5), 1505-1514. https://doi.org/10.5194/bg-7-1505-2010

Hooijer, A., Page, S., Navratil, P., Vernimmen, R., & Mawdsley, N. (2014). Carbon Emissions from Drained and Degraded Peatland in Indonesia and Emission Factors for Measurement , Reporting and Verification (MRV) of Peatland Greenhouse Gas Emissions. *Forda-Mof.Org*(May), 50-50. http://www.forda-mof.org/files/12._Carbon_Emissions_from_Drained_and_Degraded_Peatland_in_Indonesia.pdf

Hooper, A. J. (2008). A multi-temporal InSAR method incorporating both persistent scatterer and small baseline approaches. *Geophysical Research Letters*, *35*(16), L16302-L16302. https://doi.org/10.1029/2008GL034654

Howie, S. A., & Hebda, R. J. (2018). Bog surface oscillation (mire breathing): A useful measure in raised bog restoration. *Hydrological Processes*, *32*(11), 1518-1530. https://doi.org/10.1002/hyp.11622

Hoyt, A. M., Chaussard, E., Seppalainen, S. S., & Harvey, C. F. (2020). Widespread subsidence and carbon emissions across Southeast Asian peatlands. *Nature Geoscience*, *13*(6), 435-440. https://doi.org/10.1038/s41561-020-0575-4

Jones , K., Lanthier, Y., van der Voet, P., van Valkengoed, E., Taylor, D., & Fernandez-Prieto, D. (2009). Monitoring and assessment of wetlands using Earth Observation: The GlobWetland project. *Journal of Environmental Management 90*, 2154-2169. https://doi.org/10.1016/j.jenvman.20 07.07.037

Kelly, L., & Schouten, M. G. C. (2002). Vegetation. In M. G. C. Schouten (Ed.), *Conservation and restoration of raised bogs: geological, hydrological and ecological studies* (pp. 110-169). The Heritage Service of the Department of the Environment and Local Government, Ireland; Staatsbosbeheer, the Netherlands; Geological Survey of Ireland, Dublin.

Kettridge, N., Thompson, D. K., & Waddington, J. M. (2012). Impact of wildfire on the thermal behavior of northern peatlands: Observations and model simulations. *Journal of Geophysical Research: Biogeosciences*, *117*(G2), n/a-n/a. https://doi.org/10.1029/2011jg001910

Khakim, M. Y. N., Bama, A. A., Yustian, I., Poerwono, P., Tsuji, T., & Matsuoka, T. (2020). Peatland subsidence and vegetation cover degradation as impacts of the 2015 El niño event revealed by Sentinel-1A SAR data. *International Journal of Applied Earth Observation and Geoinformation*, *84*. https://doi.org/10.1016/j.jag.2019.101953

Kim, J.-W., Lu, Z., Gutenberg, L., & Zhu, Z. (2017). Characterizing hydrologic changes of the Great Dismal Swamp using SAR/InSAR. *Remote Sensing of Environment*, *198*, 187-202. https://doi.org/10.1016/j.rse.2017.06.009

Köchy, M., Hiederer, R., & Freibauer, A. (2015). Global distribution of soil organic carbon – Part 1: Masses and frequency distributions of SOC stocks for the tropics, permafrost regions, wetlands, and the world. *Soil*, *1*(1), 351-365. https://doi.org/10.5194/soil-1-351-2015

Lees, K. J., Quaife, T., Artz, R. R. E., Khomik, M., & Clark, J. M. (2018). Potential for using remote sensing to estimate carbon fluxes across northern peatlands – A review. *Science of the Total Environment*, *615*, 857-874. https://doi.org/10.1016/j.scitotenv.2017.09.103

Leifeld, J., & Menichetti, L. (2018). The underappreciated potential of peatlands in global climate change mitigation strategies /704/47/4113 /704/106/47 article. *Nature Communications*, *9*(1). https://doi.org/10.1038/s41467-018-03406-6

Marshall, C., Sterk, H. P., Gilbert, P. J., Andersen, R., Bradley, A. V., Sowter, A., Marsh, S., & Large, D. J. (2022). Multiscale Variability and the Comparison of Ground and Satellite Radar Based Measures of Peatland Surface Motion for Peatland Monitoring. *Remote Sensing*, *14*(2). https://doi.org/10.3390/rs14020336

Massonnet, D., & Feigl, K. L. (1998). Radar interferometry and its application to changes in the earth's surface. *Reviews of Geophysics*, *36*(4), 441-500. https://doi.org/10.1029/97RG03139

Millard, K., Kirby, P., Nandlall, S., Behnamian, A., Banks, S., & Pacini, F. (2020). Using Growing-Season Time Series Coherence for Improved Peatland Mapping: Comparing the Contributions of Sentinel-1 and RADARSAT-2 Coherence in Full and Partial Time Series. *Remote Sensing*, *12*(15), 2465. https://www.mdpi.com/2072-4292/12/15/2465

Millard, K., & Richardson, M. (2018). Quantifying the relative contributions of vegetation and soil moisture conditions to polarimetric C-Band SAR response in a temperate peatland. *Remote Sensing of Environment*, *206*(December 2017), 123-138. https://doi.org/10.1016/j.rse.2017.12.011

Millard, K., Thompson, D. K., Parisien, M. A., & Richardson, M. (2018). Soil moisture monitoring in a temperate peatland using multi-sensor remote sensing and linear mixed effects. *Remote Sensing*, *10*(6). https://doi.org/10.3390/rs10060903

Minasny, B., Berglund, O., Connolly, J., Hedley, C., de Vries, F., Gimona, A., Kempen, B., Kidd, D., Lilja, H., Malone, B., McBratney, A., Roudier, P., O'Rourke, S., Rudiyanto, Padarian, J., Poggio, L., ten Caten, A., Thompson, D., Tuve, C., & Widyatmanti, W. (2019). Digital mapping of peatlands - A critical review. *Earth-Science Reviews*, *196*. https://doi.org/10.1016/j.earscirev.2019.05.014

Molan, Y. E., Lu, Z., & Kim, J.-W. (2020). Influence of the Statistical Properties of Phase and Intensity on Closure Phase. *IEEE Transactions on Geoscience and Remote Sensing*, *58*(10), 7346-7354. https://doi.org/10.1109/tgrs.2020.2982062

Nesti, G., Tarchi, D., & Rudant, J.-P. (1995). Decorrelation of backscattered signal due to soil moisture changes. IEEE International Symposium on Geoscience and Remote Sensing, Firenze, Italy.

Nolan, M., & Fatland, D. R. (2003). Penetration depth as a DInSAR observable and proxy for soil moisture. *IEEE Transactions on Geoscience and Remote Sensing*, *41*(3), 532-537. https://doi.org/10.1109/tgrs.2003.809931

Nolan, M., Fatland, D. R., & Hinzman, L. (2003). DInSAR measurement of soil moisture. *IEEE Transactions on Geoscience and Remote Sensing*, *41*(12), 2802-2813. https://doi.org/10.1109/Tgrs.2003.817211

Paloscia, S., Pettinato, S., Santi, E., Notarnicola, C., Pasolli, L., & Reppucci, A. (2013). Soil moisture mapping using Sentinel-1 images: Algorithm and preliminary validation. *Remote Sensing of Environment*, *134*, 234-248. https://doi.org/10.1016/j.rse.2013.02.027

Parish, F., Sirin, A., Charman, D., Joosten, H., Minayeva, T., Silvius, M., & Stringer, L. (2008). *Assessment on Peatlands, Biodiversity and Climate Change: Main Report. Global Environment Centre, Kuala Lumpur and Wetlands International, Wageningen*.

Peng, J., Albergel, C., Balenzano, A., Brocca, L., Cartus, O., Cosh, M. H., Crow, W. T., Dabrowska-Zielinska, K., Dadson, S., Davidson, M. W. J., de Rosnay, P., Dorigo, W., Gruber, A., Hagemann, S., Hirschi, M., Kerr, Y. H., Lovergine, F., Mahecha, M. D., Marzahn, P., . . . Loew, A. (2021). A roadmap for high-resolution satellite soil moisture applications – confronting product characteristics with user requirements. *Remote Sensing of Environment*, *252*. https://doi.org/10.1016/j.rse.2020.112162

Reddy, A. D., Hawbaker, T. J., Wurster, F., Zhu, Z., Ward, S., Newcomb, D., & Murray, R. (2015). Quantifying soil carbon loss and uncertainty from a peatland wildfire using multi-temporal LiDAR. *Remote Sensing of Environment*, *170*, 306-316. https://doi.org/10.1016/j.rse.2015.09.017

Reeve, A. S., Glaser, P. H., & Rosenberry, D. O. (2013). Seasonal changes in peatland surface elevation recorded at GPS stations in the Red Lake Peatlands, northern Minnesota, USA. *Journal of Geophysical Research: Biogeosciences*, *118*(4), 1616-1626. https://doi.org/10.1002/2013JG002404

Regan, S., Flynn, R., Gill, L., Naughton, O., & Johnston, P. (2019). Impacts of Groundwater Drainage on Peatland Subsidence and Its Ecological Implications on an Atlantic Raised Bog. *Water Resources Research*, *55*(7), 6153-6168. https://doi.org/10.1029/2019WR024937

Renou-Wilson, F., Moser, G., Fallon, D., Farrell, C. A., Müller, C., & Wilson, D. (2019). Rewetting degraded peatlands for climate and biodiversity benefits: Results from two raised bogs. *Ecological Engineering*, *127*, 547-560. https://doi.org/10.1016/j.ecoleng.2018.02.014

Roulet, N. T. (2000). Peatlands, carbon storage, greenhouse gases, and the kyoto protocol: Prospects and significance for Canada. *Wetlands*, *20*(4), 605-615. https://doi.org/10.1672/0277-5212(2000)020[0605:PCSGGA]2.0.CO;2

Scheiber, R., & Moreira, A. (2000). Coregistration of interferometric SAR images using spectral diversity. *IEEE Transactions on Geoscience and Remote Sensing*, *38*(5), 2179-2191. https://doi.org/10.1109/36.868876

Schouten, M. G. (2002). *Conservation and restoration of raised bogs: geological, hydrological and ecological studies*. The Government Stationary Office.

Sowter, A., Bateson, L., Strange, P., Ambrose, K., & Fifiksyafiudin, M. (2013). Dinsar estimation of land motion using intermittent coherence with application to the south derbyshire and leicestershire coalfields. *Remote Sensing Letters*, *4*(10), 979-987. https://doi.org/10.1080/2150704X.2013.823673

Takada, M., Mishima, Y., & Natsume, S. (2009). Estimation of surface soil properties in peatland using ALOS/PALSAR. *Landscape and Ecological Engineering*, *5*(1), 45-58. https://doi.org/10.1007/s11355-008-0061-4

Tampuu, T. (2022). *Synthetic Aperture Radar Interferometry as a tool for monitoring the dynamics of peatland surface* University of Tartu].

Tampuu, T., Praks, J., Uiboupin, R., & Kull, A. (2020). Long Term Interferometric Temporal Coherence and DInSAR Phase in Northern Peatlands. *Remote Sensing*, *12*(10). https://doi.org/10.3390/rs12101566

Thollard, F., Clesse, D., Doin, M.-P., Donadieu, J., Durand, P., Grandin, R., Lasserre, C., Laurent, C., Deschamps-Ostanciaux, E., Pathier, E., Pointal, E., Proy, C., & Specht, B. (2021). FLATSIM: The ForM@Ter LArge-Scale Multi-Temporal Sentinel-1 InterferoMetry Service. *Remote Sensing*, *13*(18). https://doi.org/10.3390/rs13183734

Toca, L., Morrison, K., Artz, R. R. E., Gimona, A., & Quaife, T. (2022). High resolution C-band SAR backscatter response to peatland water table depth and soil moisture: a laboratory experiment. *International Journal of Remote Sensing*, *43*(14), 5231-5251. https://doi.org/10.1080/01431161.2022.2131478

Wagner, W., Sabel, D., Doubkova, M., Bartsch, A., & Pathe, C. (2013). the Potential of Sentinel-1 for Monitoring Soil Moisture With a High Spatial Resolution At Global Scale. *Cycle*, *2009*(November 2009), 18-20.

Wegmüller, U., Werner, C., Strozzi, T., Wiesmann, A., Frey, O., & Santoro, M. (2015). Sentinel-1 IWS mode support in the GAMMA software. 2015 IEEE 5th Asia-Pacific Conference on Synthetic Aperture Radar (APSAR),

Wegnüller, U., Werner, C., Strozzi, T., Wiesmann, A., Frey, O., & Santoro, M. (2016). Sentinel-1 Support in the GAMMA Software. *Procedia Computer Science*, *100*, 1305-1312. https://doi.org/10.1016/j.procs.2016.09.246

Werner, C., Wegmüller, U., Strozzi, T., & Wiesmann, A. (2003). Interferometric point target analysis for deformation mapping. IGARSS 2003. 2003 IEEE International Geoscience and Remote Sensing Symposium.,

Wessel, P., Luis, J. F., Uieda, L., Scharroo, R., Wobbe, F., Smith, W. H. F., & Tian, D. (2019). The Generic Mapping Tools Version 6. *Geochemistry, Geophysics, Geosystems*, *20*(11), 5556-5564. https://doi.org/10.1029/2019gc008515

Wilkinson, S. L., Tekatch, A. M., Markle, C. E., Moore, P. A., & Waddington, J. M. (2020). Shallow peat is most vulnerable to high peat burn severity during wildfire. *Environmental Research Letters*, *15*(10). https://doi.org/10.1088/1748-9326/aba7e8

Xu, J., Morris, P. J., Liu, J., & Holden, J. (2018). PEATMAP: Refining estimates of global peatland distribution based on a meta-analysis. *Catena*, *160*, 134-140.

Yu, Z., Loisel, J., Brosseau, D. P., Beilman, D. W., & Hunt, S. J. (2010). Global peatland dynamics since the Last Glacial Maximum. *Geophysical Research Letters*, *37*(13), n/a-n/a. https://doi.org/10.1029/2010gl043584

Zebker, H. A., & Villasenor, J. (1992). Decorrelation in Interferometric Radar Echoes. *IEEE Transactions on Geoscience and Remote Sensing*, *30*(5), 950-959. https://doi.org/Doi 10.1109/36.175330

Zhang, T., Zeng, Q., Li, Y., & Xiang, Y. (2008). *Study on relation between InSAR coherence and soil moisture* XXIst ISPRS Congress Technical Commission VI, Beijing, China.

Zhou, Z. (2013). *The applications of InSAR time series analysis for monitoring long-term surface change in peatlands*

Zhou, Z., Li, Z., Waldron, S., & Tanaka, A. (2016). Monitoring peat subsidence and carbon emission in Indonesia peatlands using InSAR time series. *International Geoscience and Remote Sensing Symposium (IGARSS)*, *2016-November*, 6797-6798. https://doi.org/10.1109/IGARSS.2016.7730774

Zwieback, S., Hensley, S., & Hajnsek, I. (2015a). Assessment of soil moisture effects on L-band radar interferometry. *Remote Sensing of Environment*, *164*, 77-89. https://doi.org/10.1016/j.rse.2015.04.012

Zwieback, S., Hensley, S., & Hajnsek, I. (2015b). A Polarimetric First-Order Model of Soil Moisture Effects on the DInSAR Coherence. *Remote Sensing*, *7*(6), 7571-7596. https://doi.org/10.3390/rs70607571

Zwieback, S., Hensley, S., & Hajnsek, I. (2017). Soil Moisture Estimation Using Differential Radar Interferometry: Toward Separating Soil Moisture and Displacements. *IEEE Transactions on Geoscience and Remote Sensing*, *55*(9), 5069-5083. https://doi.org/10.1109/tgrs.2017.2702099

List of figures:

List of tables: